Advances in Water Resources 209 (2026) 105217

Contents lists available at ScienceDirect

Advances in Water Resources

journal homepage: www.elsevier.com/locate/advwatres

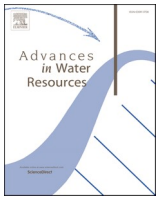

Capturing scales of heterogeneity in models of fluvial geothermal reservoirs: Grid resolution, upscaling strategies, and hierarchies of sedimentary architecture

Hamed Aghaei [a,*], Luca Colombera [a], Na Yan [b], Nigel P. Mountney [b], Odd Andersen [c], Andrea Di Giulio [a]

[a] Dipartimento di Scienze della Terra e dell'Ambiente, Università di Pavia, Italy
[b] School of Earth & Environment, University of Leeds, UK
[c] SINTEF Digital, Dept. of Mathematics and Cybernetics, Norway

ARTICLE INFO

Keywords:
Low-enthalpy geothermal
Sedimentary heterogeneity
MODFLOW
MT3D-USGS
Fluvial succession

ABSTRACT

This study investigates the influence of modeling choices related to the scale of reservoir heterogeneity on the predicted performance of geothermal doublets in fluvial low-enthalpy geothermal reservoirs. Fourteen geocellular grids were created to systematically analyze the impacts of numerical grid resolution, permeability upscaling methodology, and modeled scales of sedimentary architecture, using MODFLOW-2005 and MT3D-USGS to simulate groundwater flow and heat transport for well-doublet operation over a 35-year period. The results reveal complex relationships between these choices and simulated reservoir behavior: the considered factors have significant influence on injection pressures but only a modest effect on production temperatures (with variations within 2 °C after 35 years across all models), likely due, at least in part, to a relative dominance by thermal diffusion over heat advection in the considered scenarios. Simplification of geological architecture through omission of fine-scale features may augment the hydraulic impact of larger flow barriers, such as abandoned-channel mud plugs. The highest injection pressures were simulated on grids that embody sedimentary architectural elements but lack internal facies heterogeneity. The permeability upscaling method also has an effect: simulations on grids upscaled using harmonic averaging consistently yield the highest near-injector pressures, followed by those based on geometric averaging and arithmetic averaging. The dynamic behavior of grids upscaled via flow-based upscaling closely approximates that of grids upscaled using arithmetic averaging, suggesting that bulk hydraulic behavior is dominated by the connectivity of high-permeability units. The performance gap between grids following different upscaling methods decreases significantly for higher grid resolution. Simulations of geological models that incorporate increasingly detailed geological features predict cold-water plumes with slightly more complex shapes and tortuous fronts, as documented by values of plume surface-to-volume ratio. The complexity of the cold-water plume shape, as measured by the surface-to-volume ratio, is slightly higher for well doublets oriented at a high angle to the channel-belt axis, but does not increase systematically with the resolution at which fine-scale features are represented.

1. Introduction

To reliably forecast the pressure and temperature evolution of geothermal reservoirs, it is crucial that the static models that underpin numerical simulations incorporate geological, petrophysical and thermal properties realistically (Hamm and Lopez, 2012; Vogt et al., 2013; Wang et al., 2023; Willems et al., 2017b). Yet building geologically robust reservoir models remains challenging. Fully resolving subsurface complexity often requires static grids with millions of cells, each assigned properties via geostatistical or process-based methods (Feyen and Caers, 2006; Janssen et al., 2006). Although such fine resolution is computationally expensive, coarser-grid models may fail to capture key geological heterogeneities, whose impact may not be accounted for by standard upscaling techniques (Renard and de Marsily, 1997). If grid cell dimensions do not match with the length scales of depositional or diagenetic features, cell-to-cell property contrasts may reflect numerical

* Corresponding author.
E-mail address: hamed.aghaei@unipv.it (H. Aghaei).

https://doi.org/10.1016/j.advwatres.2026.105217
Received 20 October 2025; Received in revised form 12 January 2026; Accepted 12 January 2026
Available online 21 January 2026

artifacts rather than true heterogeneity (Nordahl and Ringrose, 2008). To facilitate the simulation of large-scale models, heterogeneous property fields are usually upscaled. Arithmetic, harmonic and geometric averaging approaches are variably applied depending on the architecture of geological media; however, none of these may be suited to more complex architectures, for which local flow-based techniques or multi-scale finite-volume methods may be preferred (Renard and de Marsily, 1997; Jenny et al., 2003). Additional challenges exist in the upscaling of petrophysical properties for multiphase or heat-transport problems, whereby pseudo-relative-permeability functions and macro-dispersion tensors must preserve sub-grid physics (Barker and Thibeau, 1997; Chen et al., 2003).

Numerous studies have documented ways in which sedimentary heterogeneity governs flow paths, breakthrough timing and sweep efficiency in both geothermal and hydrocarbon reservoirs (Lake and Jensen, 1991; Gómez-Hernández and Wen, 1998; Graham et al., 2015). Heterogeneity arises from sedimentary architecture and diagenetic products, which cause permeability and porosity to vary over orders of magnitude (Jackson et al., 2003; Aghaei et al., 2024). Neglecting complexities, such as the presence of sedimentary units that act as thief zones leading to premature thermal breakthrough, poses risks in the intended use of reservoir models (Ringrose and Bentley, 2016). Recent studies based on outcrop analogs and forward-stratigraphic modeling of fluvial successions highlight the role of point-bar and channel-belt architectures in controlling geothermal well-doublet performance (Babaei and Nick, 2019; Major et al., 2023; Aghaei et al., 2024).

The extraction of heat from low-enthalpy geothermal reservoirs is commonly performed employing multi-well schemes – such as doublets (Gringarten, 1978; Mahbaz et al., 2021) or triplets (Chen and Jiang, 2015; Zinsalo et al., 2021); for these, optimal well spacing and orientation dictate longevity and efficiency of operation, but their choice depends on the specifics of reservoir architecture and heterogeneity. Numerical studies demonstrate how the optimization of doublet design and operation is strongly dependent on geological architecture and heterogeneity (Daniilidis et al., 2020; Ezekiel et al., 2022; Kong et al., 2017).

Consideration of how geological heterogeneities are represented and upscaled in geothermal reservoir models is especially important in clastic sedimentary aquifers. One such class of aquifers is represented by sedimentary successions produced by meandering river systems, in which sedimentary units are arranged in a predictable hierarchical manner (Fig. 1; cf. Tyler and Finley, 1991; Miall, 2014). These units include large-scale depositional elements consisting of meander-belt channel bodies representing the principal target sand bodies in successions of this type (Gibling, 2006); these channelized units are commonly embedded in fine-grained floodplain deposits (Ghinassi and Ielpi, 2015). Internally, fluvial channel bodies are composed of architectural elements that typically comprise sand-prone point-bar elements compartmentalized by mud-prone abandoned-channel-fill elements (Donselaar and Overeem, 2008; Colombera et al., 2017). At a smaller scale,

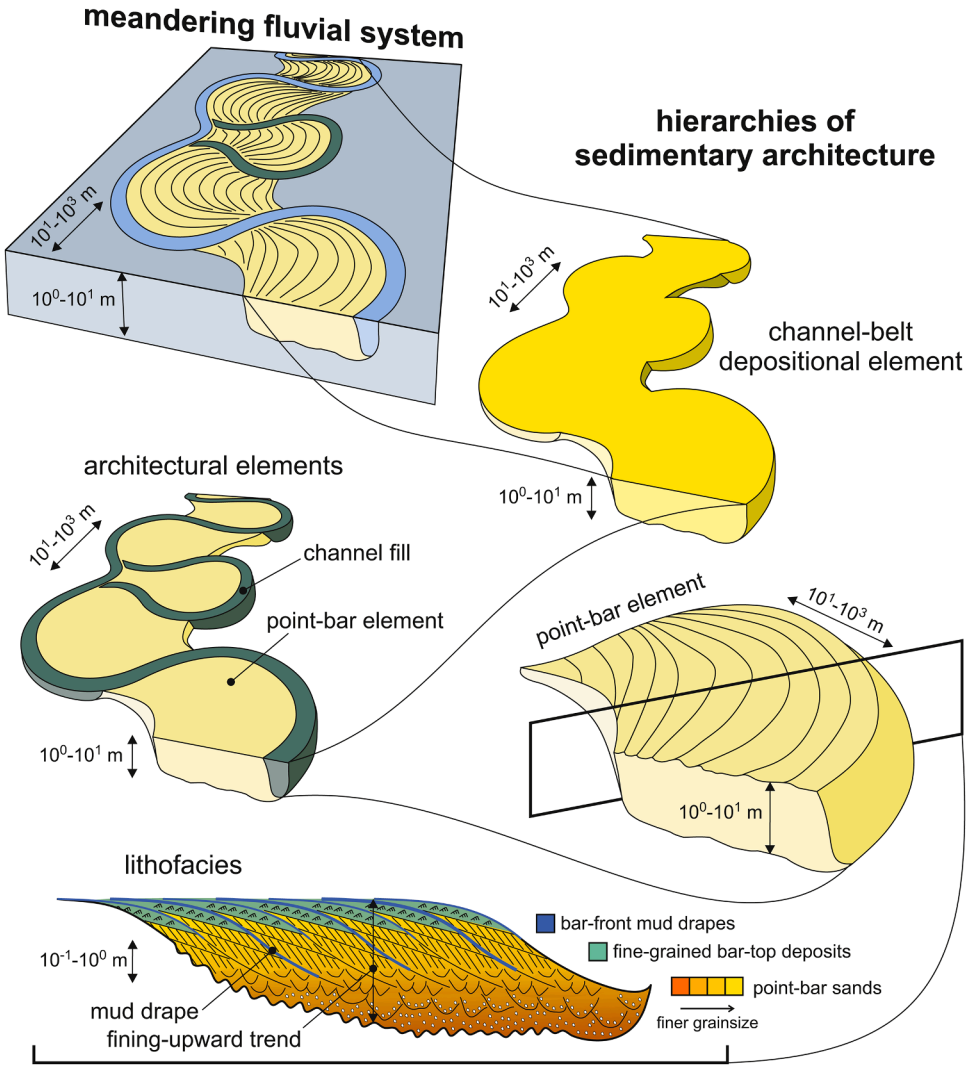

Fig. 1. Idealized models depicting the scales of sedimentary heterogeneity of meander-belt successions considered in this study.

meander-belt architectural elements are made of lithofacies units representing the preserved record of specific depositional and post-depositional processes, giving rise to significant internal variability in grain-size, continuity and connectivity of net reservoir volumes (Bridge, 2003; Russell et al., 2019). All these scales of heterogeneity control fluid flow in the successions of meandering rivers (cf. Montero et al., 2024; Willis and Sech, 2019).

The aim of the present work is to determine the importance of capturing scales of sedimentary heterogeneity in the practice of modeling fluvial low-enthalpy geothermal reservoirs. Specific objectives include the systematic quantification of the impacts of (i) numerical-grid resolution, (ii) upscaling methodology, and (iii) hierarchical scales of fluvial sedimentary architecture on the performance of geothermal doublets in meander-belt reservoirs. This assessment seeks to deliver practical guidelines that may be followed to make informed choices of geocellular grid resolution and permeability upscaling strategies. Although the numerical tools for flow simulation and upscaling are well-established, their application to the specific challenges of low-enthalpy geothermal reservoirs hosted in heterogeneous sedimentary aquifers remains under-explored. The novelty of this work lies in the systematic, structured comparison of these modeling choices.

2. Methodology

This work employed a numerical model named Point-Bar Sedimentary Architecture Numerical Deduction (PB-SAND) (Yan et al., 2021, 2017), to construct vector-based representations of meander-belt fluvial deposits. The resulting idealized architecture was voxelized into a geocellular grid that captures different levels of sedimentary heterogeneity: (i) depositional elements including a channel belt and the floodplain deposits in which it is embedded, (ii) channel-belt components consisting of barform and channel-fill architectural elements, and (iii) the lithofacies types that make up the point-bar and channel-fill elements (Fig. 1); these units can be selectively activated or omitted. In this geological framework, petrophysical properties were then populated through geostatistical methods. Starting from a highest-resolution grid, equivalent static models of progressively coarser resolution were obtained through upscaling along a specified horizontal axis, preserving the same architectural framework at each scale. These grids were then subsequently used as static meshes for simulating water flow and heat transport in an idealized low-enthalpy geothermal reservoir. Fig. 2 summarizes the modeling workflow undertaken in this work.

2.1. Reservoir modeling

A three-dimensional geocellular grid consisting of 1750 × 104 × 52 cells was built to depict a sand-prone fluvial meander-belt succession produced by a chiefly downstream-migrating (translating) meandering river channel. As detailed in a companion paper by Aghaei et al. (2024), the model captures key characteristics of the facies architecture of meander belts: fine-grained abandoned channel fills, upward-fining sequences, a planform grain-size trend whereby downstream point-bar tails are finer-grained than their upstream correlative bar heads, and mud layers that locally drape point-bar accretion surfaces (Fig. 3; Pranter et al., 2007; Colombera et al., 2018; McGowen and Garner, 1970; Hartkamp-Bakker and Donselaar, 1993; Alsop et al., 2014).

The depositional architecture was generated with the PB-SAND forward model (Yan et al., 2017, 2021). This computer program traces time-stamped channel-centerline trajectories in vector space, calculating bank erosion and lateral-accretion geometries before any discretization in gridded format occurs, so that even very thin inclined beds (e.g. bar-front mud drapes) are not aliased at export and are thereby preserved as part of the model outputs. Lithological facies types are then distributed according to rules that consider geological understanding of the processes determining their distribution in meander-belt elements, for example, the position of point-bar and counter-point-bar deposits (Yan et al., 2021); these facies units are parameterized in terms of proportions and geometries. The reference model was created using input channel trajectories that describe meander-belt evolution associated with dominant meander-bend translation (Aghaei et al., 2024); it covers an area of 5382 × 4784 m^2 and has a vertical extent of 10 m. This thickness was chosen to capture the full preserved vertical thickness of a single meander-belt depositional element representative of the successions of mid-sized river systems (Blum et al., 2013; Colombera et al., 2019; Gibling, 2006). The resulting vector model was discretized into a cartesian geocellular grid. Facies-controlled porosity and permeability were populated with collocated sequential Gaussian co-simulation (SGCoSim) in SGeMS 3.0. The algorithm SGCoSim (Almeida and Journel, 1994) preserves both the individual variograms of each property and their cross-correlation. Prior distributions came from data obtained from geological analogs (Aghaei et al., 2024). Dimensional and hierarchical rules (e.g., typical barform thicknesses, mud-drape spacing) were sampled from the Fluvial Architecture Knowledge Transfer System (FAKTS), a sedimentological database collating data from fluvial depositional systems (Colombera et al., 2012). Point-bar–scale porosity-permeability ranges were calibrated against outcrop-derived

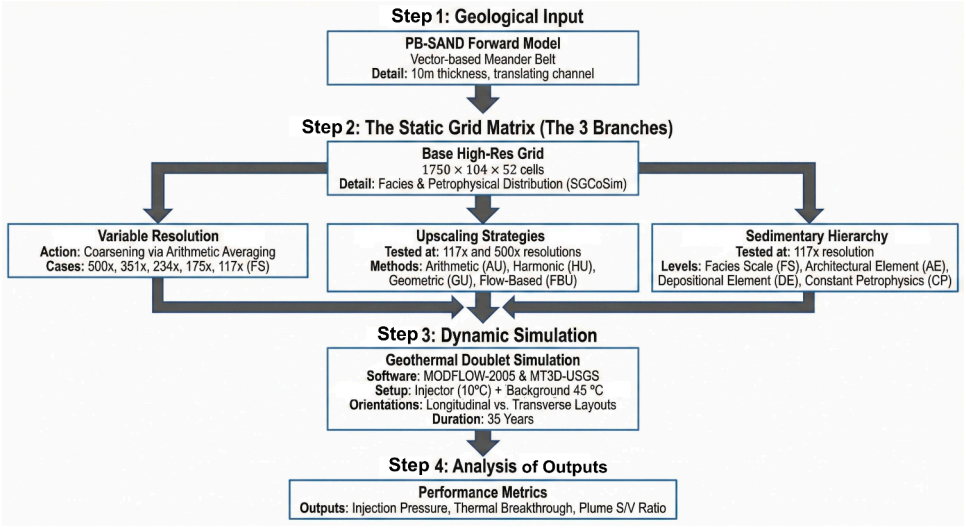

Fig. 2. Overview of the modeling workflow followed in this study.

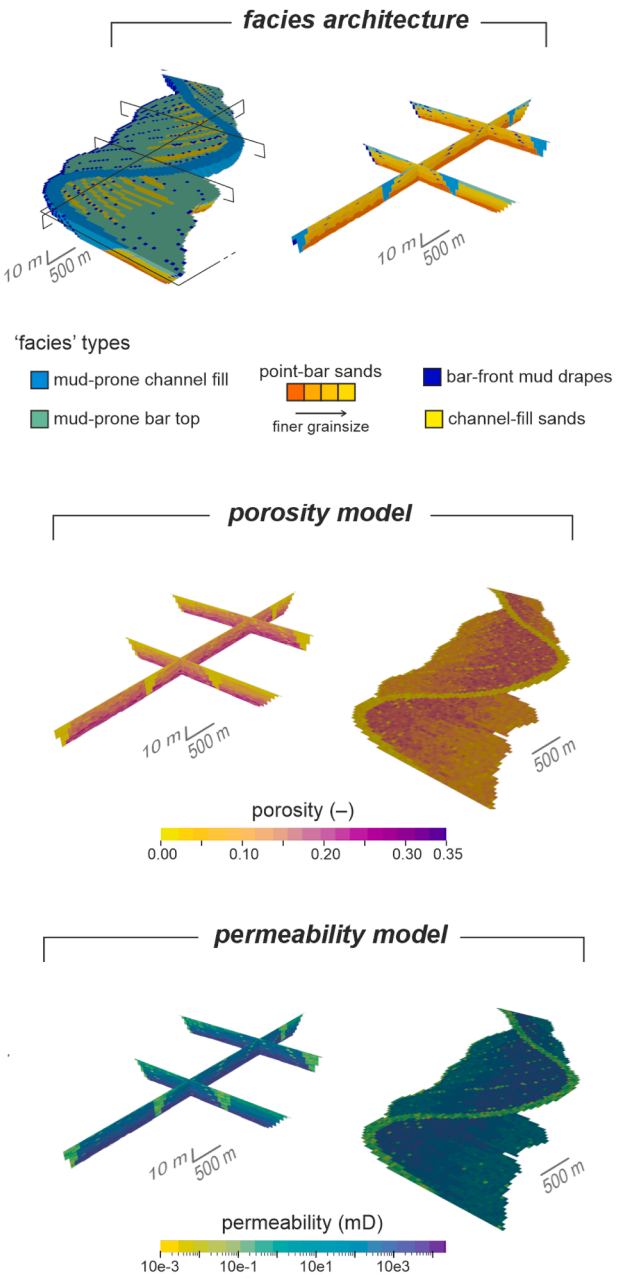

Fig. 3. Plan-view and vertical cross-sectional views of the base-case grid considered in this study, showing facies distributions, porosity, and permeability (adapted from Aghaei et al., 2024).

compilations that document intra-bar heterogeneity and its impact on fluid flow (Willis and Sech, 2019).

2.2. Upscaling of petrophysical properties: approaches and cell sizes

To isolate the controls of (i) grid resolution, (ii) permeability upscaling technique, and (iii) sedimentary-heterogeneity hierarchy on geothermal doublet behavior, we generated a suite of geocellular models from the PB-SAND base grid. The base grid (1750 × 104 × 52 cells) was coarsened along a single specified direction ('x' direction, i.e., the horizontal direction at higher angle with the direction of elongation of the modeled channel-belt depositional element) by arithmetic averaging so that six alternative grids of varying resolution were produced, respectively having 500, 351, 234, 175, and 117 cells along the x direction. All these grids have a y-direction resolution of 104 cells and a vertical resolution of 52 cells. The base grid was intentionally coarsened along the 'x' direction only. This was done to isolate the effect of grid resolution and upscaling for a specific direction, noting that channel-belt heterogeneities are intrinsically anisotropic and considering that two alternative well-doublet layouts are simulated that are variably oriented relative to the direction of channel-belt elongation.

Since all these grids incroporate facies-scale heterogeneity, they are denoted by the 'FS' acronym, and are hence labelled as: 500x-FS, 351x-FS, 234x-FS, 175x-FS, and 117x-FS (Fig. 4). These grids preserve the general architectural characteristics of PB-SAND outputs, allowing us to examine the impact of one-directional grid coarsening on simulated fluid flow and heat transport.

For each of two selected grid resolutions (500 and 117 cells along x direction), three additional grids were created by performing permeability upscaling using harmonic averaging, geometric averaging, and a flow-based approach. Arithmetic block averaging was used for upscaling porosity values in all cases. The resulting five grids are denoted as 500x-HU-FS,117x-HU-FS, 500x-GU-FS, 117x-GU-FS, 500x-FBU-FS and 117x-FBU-FS depending on whether upscaling is based on harmonic averaging (HU), geometric averaging (GU) or flow-based upscaling (FBU). In the flow-based upscaling workflow, the effective permeability value for each cell was determined by imposing a pressure drop and simulating the resulting flow using the functionality of the upscaling module of the Matlab Reservoir Simulation Toolbox (MRST; Lie, 2019; Lie and Møyner, 2021). This was repeated for each of the three cartesian axes. A full permeability tensor was computed considering no-flow conditions applied to the lateral boundaries. The total computing time required to perform flow-based upscaling was up to a maximum of ca. 380 h for the grid at 117x resolution, using a standard desktop PC with 32 GB RAM and Intel Core i7 CPU. The standard Layer-Property Flow (LPF) package in MODFLOW-2005 assumes that principal hydraulic conductivity axes align with the model grid; thus, only the diagonal components of the upscaled tensor (K_{xx}, K_{yy}, K_{zz}) were extracted and used for the dynamic simulations. Disregarding the off-diagonal terms is justified by the fact that the grid axes are oriented to align approximately with the principal directions of depositional anisotropy.

Together with grids of the same resolutions but obtained via arithmetic averaging, these grids enable a comparison of predicted reservoir behavior as a function of permeability upscaling technique.

2.3. Hierarchies of sedimentary heterogeneity

To assess the impact of different hierarchical levels of sedimentary architecture on doublet performance, additional grids were built at a common resolution of 117 × 104 × 52; these grids differ with respect to the domains and manner in which petrophysical properties are assigned (Table 1, Fig. 5; see also Fig. 1). A grid denoted as 117x-AE has been obtained by distributing petrophysical properties, via SGCoSim (Almeida and Journel, 1994), in a simplified lithological framework in which point-bar and abandoned-channel-fill architectural elements are differentiated but their internal facies heterogeneity is ignored. A grid denoted as 117x-DE has been obtained by considering a lithological framework that is simplified even further: porosity and permeability modeling is performed in the channel-belt domain without any form of facies constraint. An additional grid denoted as 117x-CP has been produced by setting all channel-belt deposits as having constant values of porosity and permeability.

2.4. Hydrogeological modeling and heat-transport simulation

The numerical workflow used in this work follows closely the one documented in Aghaei et al. (2024). Groundwater flow is solved with MODFLOW-2005 (Harbaugh, 2005), whereas coupled heat transport by advection and conduction is simulated in MT3D-USGS (Bedekar et al., 2016) through the Advection (ADV) and Dispersion (DSP) packages. Dispersivity was set to zero because, for the facies-scale models

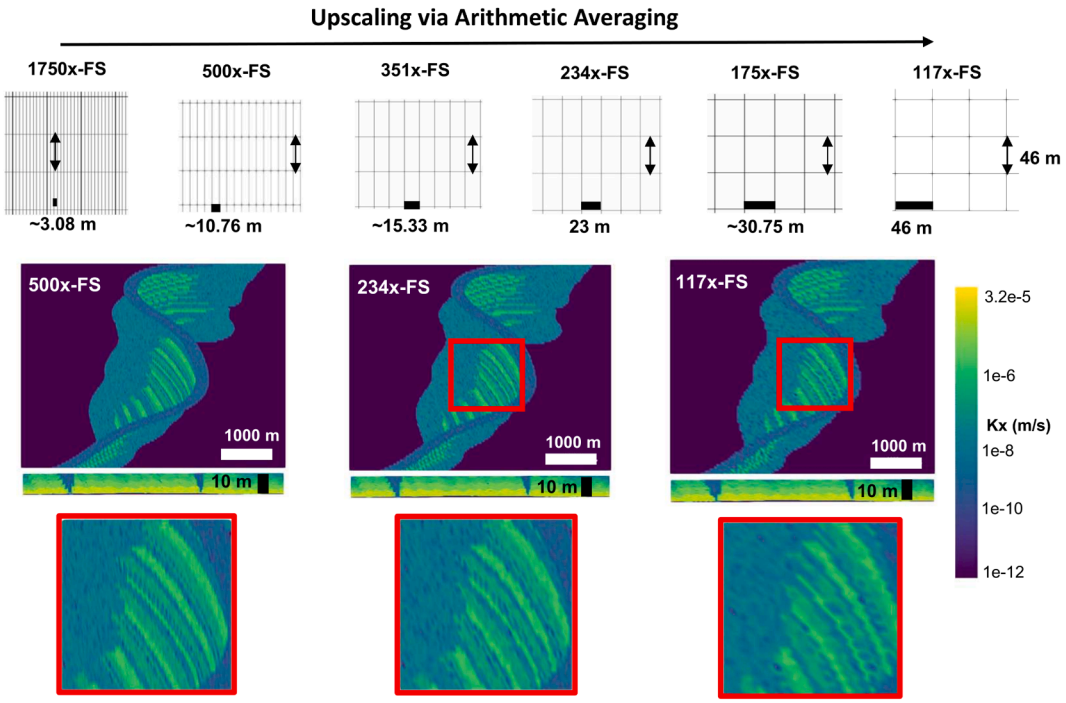

Fig. 4. Schematic representation of the considered grid resolutions accompanied by selected plan-view and cross-sectional slices color-coded by hydraulic conductivity (Kx, m/s), highlighting the spatial arrangement of facies types controlling petrophysics; upscaling of both porosity and permeability was performed via arithmetic averaging for these grids.

Table 1
Summary of grids built to assess the impact of hierarchies of sedimentary heterogeneity on doublet performance.

Grid	Grid code	Heterogeneity domains used for geostatistical modeling
Facies-scale	117x-FS	Lithofacies units distributed in the architectural elements of the meander-belt depositional element
Architectural-Element scale	117x-AE	Point-bar and channel-fill architectural elements making up the meander-belt depositional element
Depositional-Element scale - Gaussian Petrophysics	117x-DE	Undifferentiated meander-belt depositional element; Gaussian distributed porosity and permeability values
Depositional-Element scale - Constant Petrophysics	117x-CP	Undifferentiated meander-belt depositional element; constant porosity and permeability values reflecting depositional-element mean values

considered here, spatial variability in hydraulic conductivity already captures mechanical dispersion at the grid scale (Ferguson, 2007; Sommer et al., 2013). In practical real-world applications based on standard hydrogeological modeling of aquifer models, dispersivity would not normally be set to zero. Negligible dispersivity values may only be appropriate for very high-resolution representations of aquifer heterogeneity (Possemiers et al., 2015); this choice was adopted here in all cases for consistency in order to isolate the influence of other parameters on model outputs. This ensures that the observed mixing is primarily a function of the explicit geological architecture and numerical dispersion inherent to the finite-difference method.

Saturated flow was simulated using the Layer-Property Flow (LPF) package; regional inflow/outflow was represented with General-Head Boundaries (GHB). A constant background temperature was set to 45 °C in line with the idealized scenarios simulated in Aghaei et al. (2024). Operation of the well doublet was implemented with the Multi-Node Well package (MNW2), considering injection of 10 °C water at 0.003 $m^3 s^{-1}$ and variable production at reservoir conditions. Values of thermal conductivity and heat capacity were separately assigned for sand- and mud-dominated facies following analog data compiled by Dalla Santa et al. (2020). Bulk thermal diffusion is calculated cell-by-cell based on the local porosity values.

Unlike permeability, which exhibits variation over several orders of magnitude in the considered fluvial facies (ranging from approximately 1.00E-12 to 3.20E-05 m/s), thermal conductivity varies within a much narrower range (approximately by a factor of 1.5 to 2 between sand and mud). Consequently, arithmetic (volume-weighted) averaging was applied to upscale all petrothermal properties in this work. It has been demonstrated by Rühaak et al. (2015) that, for layered sedimentary formations, upscaling approaches based on harmonic or geometric averaging often reproduce fine-scale values more accurately than arithmetic averaging, but it is also recognized that the specific upscaling method has a relatively minor impact on the resulting temperature distribution due to the diffusive nature of heat conduction .

Each scenario is simulated for 35 years, with hydrogeological and thermal inputs summarized in Table 2-Appendix A.

2.5. *Well-doublet layouts*

Two geothermal doublet arrangements were analysed that differ in how they align with the meander-belt axis (Fig. 6); these are indicated as: (i) “longitudinal” layout when the producer and injector are placed along the direction of elongation of the meander-belt (approximately along the average river paleoflow), i.e., at high angle with the direction of grid coarsening; (ii) “transverse” layout when the wells are oriented at high angle with the axis of the channel belt, i.e., at low angle with the direction of grid coarsening. Point-bar accretions surfaces, and the bar-front mud drapes that mantle some of these surfaces, strike roughly parallel to the transverse layout. In both cases the inter-well distance is fixed at 1050 m. To avoid lack of well communication due to hydraulic barriers associated with abandoned-channel mud plugs, the screened intervals of both wells are set to penetrate the same point-bar architectural element. Hydraulic heads are specified so that the injector is

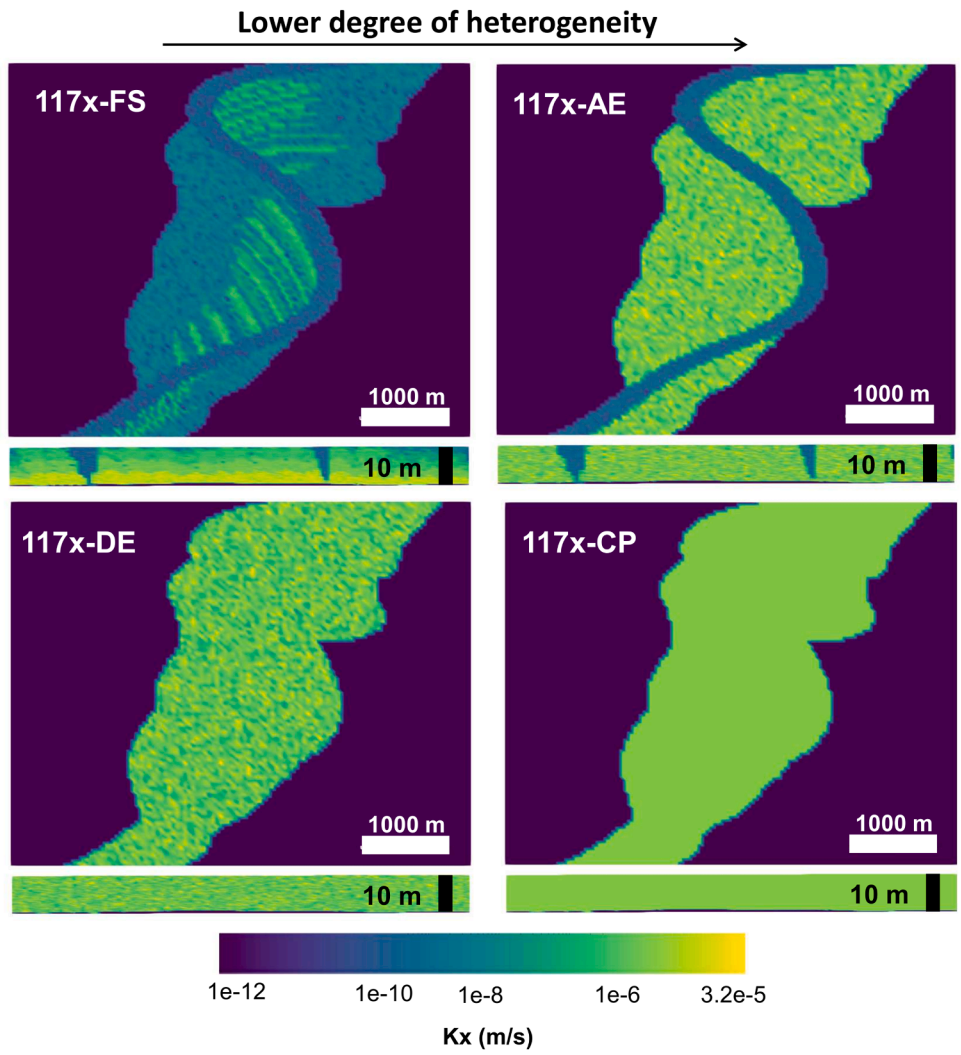

Fig. 5. Plan-view and cross-sectional views of grids that differ in the degree with which hierarchies of sedimentary architecture are considered, color-coded by hydraulic conductivity (Kx, m/s) highlighting the spatial arrangement of hierarchies of sedimentary heterogeneity, or lack thereof, at 117×104×52 resolution.

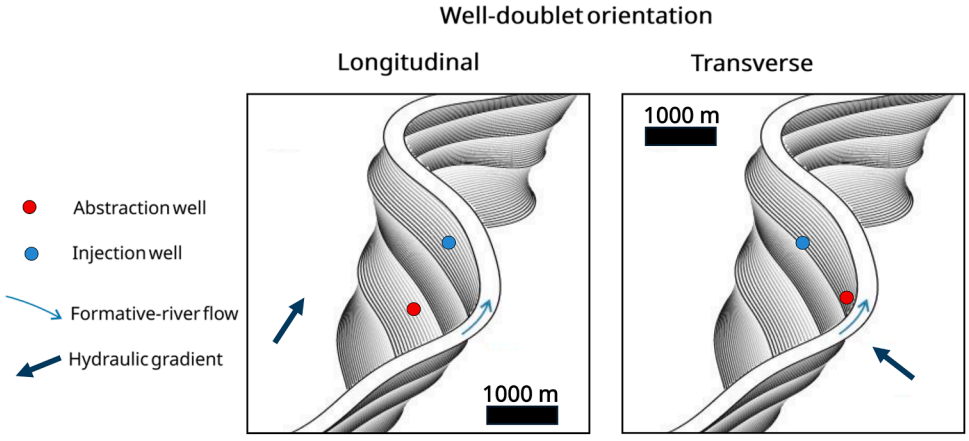

Fig. 6. Map view of longitudinal and transverse well-doublet configurations used in this work with well spacing of 1050 m.

positioned down-gradient of the producer, a standard practice aiming to delay thermal breakthrough (Banks, 2009).

2.6. Surface-to-volume ratios (S/V)

The ratio between the surface area and the volume of an object can be considered as a measure of its tortuosity (cf. Deutsch, 1998). In the case of injected cold-water plumes, this metric is affected by the way in

which the plume is defined. The definition is important if the interest is specifically on the tortuosity of flow, due to the influence of heat conduction on plume shape. In the current work, plumes are defined from the 3-D temperature field at 35 years by thresholding at T* in the range 10–20 °C. For a given T*, the plume volume (V) is the sum of the native grid-cell volumes with $T \leq T^*$; the plume surface (S) is estimated as the total area of cell faces separating plume and non-plume cells.

To evaluate the petrophysical heterogeneity of each grid, two scalar descriptors are used: (i) the porosity coefficient of variation (CV_Φ), a dimensionless measure of porosity spread defined as $CV_\Phi = \sigma / \mu$, where σ is the porosity standard deviation and μ the mean porosity, such that larger CV_Φ values indicate greater porosity heterogeneity; (ii) the Dykstra–Parsons coefficient (VDP), a measure of permeability heterogeneity (Dykstra and Parsons, 1950) defined as: VDP = $[\log k_{50} - \log k_{84.1}] / \log k_{50}$, where k_{50} and $k_{84.1}$ are the 50th and 84.1st percentiles of the permeability distribution, respectively, such that a higher VDP signifies more pronounced permeability heterogeneity.

3. Results

3.1. Geocellular grids: comparison of petrophysical heterogeneity

Together, the fourteen geocellular models considered in this work permit an analysis of the relative influence of resolution, upscaling method, and complexity in sedimentary architecture on the predicted fluid flow and heat transfer of a geothermal doublet.

Fig. 7 provides a summary comparison in the form of porosity-permeability plots charting values for all the cells of grids that differ in terms of resolution and permeability upscaling approach (arithmetic, harmonic and geometric averaging and flow-based upscaling). Arithmetic upscaling largely preserves the distinct high-density clusters representing the transition from sand-prone to mud-prone facies, with the CV_Φ remaining stable at 0.42 and the VDP at 0.16. The plots for grids upscaled using HU show a marked shift in the data distribution compared to the arithmetic baseline. This occurs because the harmonic mean is sensitive to low values, causing a suppression of effective permeability in heterogeneous cells and resulting in a different clustering pattern. In contrast, the GU plots display an intermediate trend; while they retain the general shape, the geometric mean tends to reduce the influence of extreme high-permeability values compared to arithmetic averaging. Finally, the FBU plots for the 500x resolution reveal significant scatter, particularly in the vertical direction (kz). Unlike the static averaging methods, flow-based upscaling captures the directional anisotropy induced by the geological architecture, resulting in a higher VDP (0.26 for kz) that reflects the flow barriers presented by mud drapes and baffles.

Fig. 8 shows corresponding plots for grids that differ in terms of degrees of considered sedimentary heterogeneity. The plot for the 117x-FS (Facies-Scale) grid displays a continuous, curvilinear trend with high-density clusters, representing the highest level of geological detail

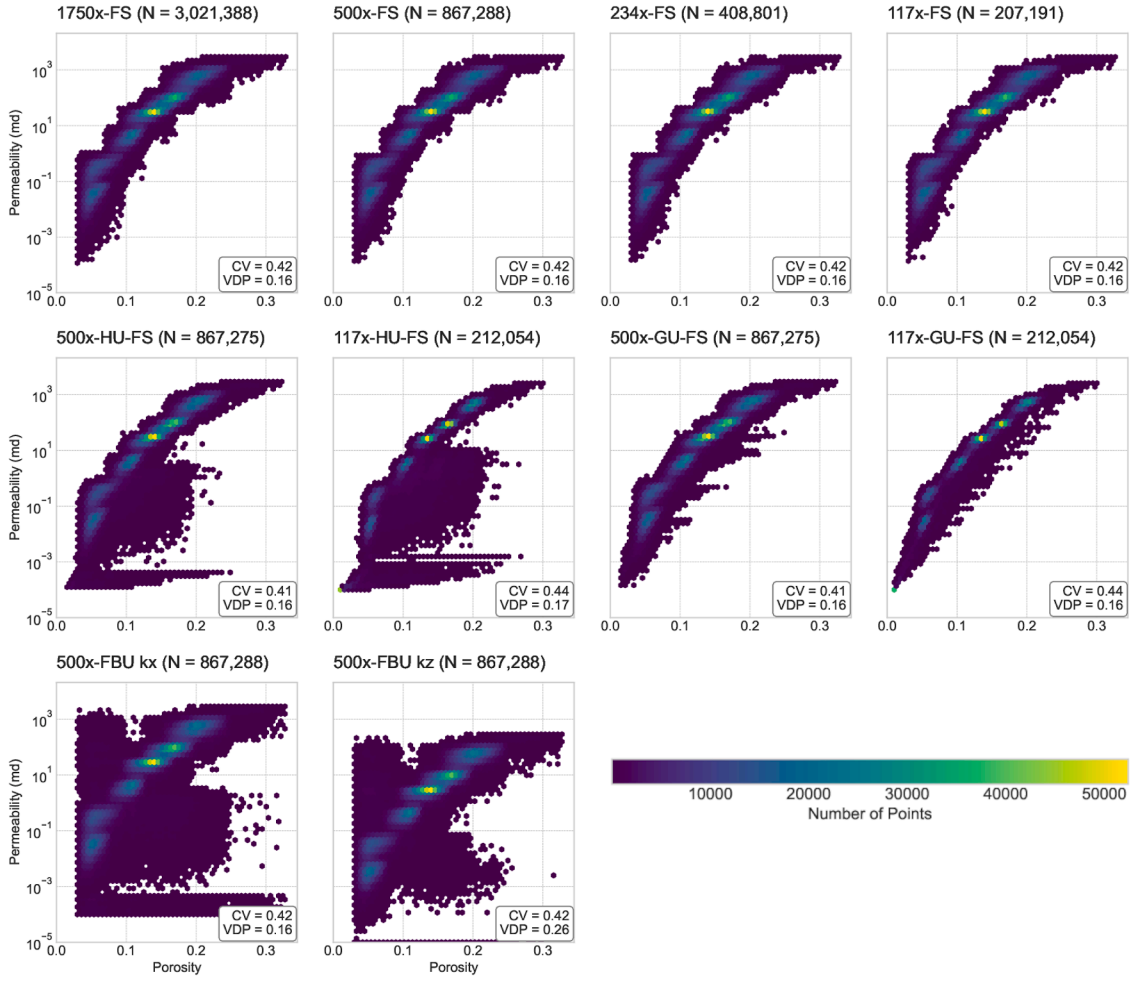

Fig. 7. Cross plots of porosity and permeability values for cells of selected grids of variable resolution and for which permeability values were upscaled using arithmetic, harmonic and geometric averaging methods or a flow-based upscaling technique. Values of porosity CV_Φ and Dykstra–Parsons coefficient (VDP) for each grid are reported. N: number of data points; kx, ky and kz: Permeability in x, y and z directions. Note that the 1750x-FS grid is shown for reference as the finest-scale model, but was not used in the dynamic simulations due to computational limitations.

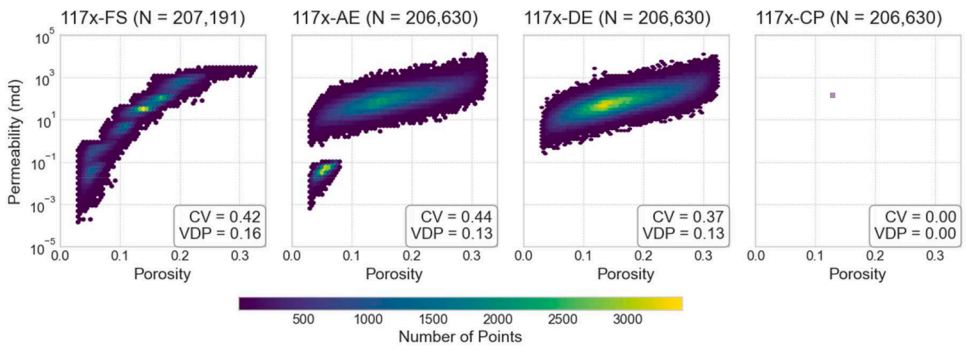

Fig. 8. Cross plots of porosity and permeability values for cells of grids that consider different levels of sedimentary heterogeneity (see Table 1). The values of porosity CV_ϕ and Dykstra–Parsons coefficient (VDP) are reported for each grid.

examined. This "S-shaped" distribution reflects the preservation of facies-scale heterogeneity, where distinct lithofacies units—such as channel sands, bar-top deposits, and mud drapes—are arranged according to realistic depositional trends. The trend effectively captures the intrinsic cross-correlation between porosity and permeability defined by the underlying geostatistical rules, bridging high-quality reservoir sands with lower-quality heterolithic and muddy facies. In contrast, the 117x-AE grid exhibits two distinct, disconnected data clouds, indicating a bimodal distribution caused by simplifying the geology to the architectural-element scale. By treating sand-prone point bars and mud-prone abandoned channel fills as internally homogeneous units, this model ignores the facies that would naturally connect them. The resulting gap between the upper and lower clouds highlights the artificial binary classification of rock types at this scale, effectively removing the deposits that usually bridge clean sands and mud plugs. Moving to a lower level of detail, the 117x-DE grid presents a single, diffuse, and broad cloud of data points. This occurs because the model treats the entire meander belt as one undifferentiated depositional element, populating porosity and permeability using a Gaussian distribution across the domain without facies or architectural constraints. Consequently, the petrophysical properties are "smeared" into a structureless blob, mixing high and low values randomly rather than organizing them according to specific depositional processes or boundaries. Finally, the 117x-CP grid collapses the entire dataset into a single point on the cross-plot. This represents the most extreme simplification, where all spatial heterogeneity is removed by assigning a constant mean value for porosity and permeability to every cell within the depositional element.

3.2. Impact of grid resolution

For both longitudinal and transverse well-doublet layouts, the choice of grid resolution has a relatively modest influence on the local injection-well pressure and on the inter-well pressure difference (|Δ Head|); also, variations in the pressure field are not seen to arise systematically as a function of cell size (Fig. 9a-b). Differences in production temperatures (Fig. 9c-d), which reflect changes in the rate of advance of the cold-water front through the point-bar sand body, are also very limited, falling within ca. 1 °C at any point in time across all grids for a given doublet layout. This is likely due, at least in part, to a relative dominance by thermal diffusion over heat advection in the considered scenarios. This behavior reflects a low Péclet number (P_e)—the dimensionless ratio of advective to diffusive heat transport—inherent to the chosen flow rate of 0.003 m^3/s. In this low-flow scenario, the smoothing effect of heat conduction across facies boundaries partially masks the impact of architectural heterogeneity on heat propagation. Also abstraction temperatures do not vary systematically with the grid resolution. Overall, progressive grid refinement does not yield a monotonic trend in either injector pressure or production temperature over 35 years; the highest injector pressures are simulated using the 234x-FS grid for both layouts (Fig. 9e-f). A careful visual inspection of plume propagation in plan-view maps and cross-sections was carried out to seek an explanation for these observations, revealing that there appears to be no evident geological control; thus, we interpret this behavior as a resolution-dependent numerical effect requiring targeted sensitivity tests (advection scheme, timestep size, solver tolerances, and alternative upscaling).

A striking result from the analysis of the effects of grid resolution is the observation of the highest near-injector pressures in simulations run on the intermediate-resolution 234x-FS grid (Fig. 9e). While monotonic convergence is typically expected in homogeneous media, this non-monotonic behavior highlights a critical 'discretization trap' specific to high-contrast heterogeneities (e.g., sand vs. mud). It is possible that at coarse resolutions (117x) numerical dispersion is dominant; the distinct hydraulic resistance of mud drapes is 'smeared' out by the finite-difference approximation, artificially enhancing connectivity and lowering pressure. As resolution increases to intermediate levels (234x), numerical dispersion may be reduced, allowing mud drapes to act as ‘sharp’ barriers. However, such a grid may not be sufficiently fine to resolve the complex flow pathways that exist around these barriers. This underscores the necessity of conducting targeted grid-sensitivity studies that go beyond simple convergence checks, particularly in facies-based models where high permeability contrasts exist.

3.3. Impact of sedimentary heterogeneity hierarchy

Across the four grids considered for evaluating the impact of the scale at which sedimentary heterogeneity is considered (Table 1), it is observed that the simulated near-injector pressure build-up and the well pressure differences evolve in markedly different ways (Fig. 10a-b), but not systematically in relation to the degree of incorporated heterogeneity. For example, the highest injection pressures are simulated for the longitudinal layout on the architectural-element scale grid (117x-AE), which may reflect the increased influence of the channel-abandonment mud plug as a flow barrier; in turn this is shown to have had an effect on the asymmetry of propagation of the cold-water plume in absence of facies-scale heterogeneities (Fig. 10c-d). Variations in the rates of temperature decline at the production well (Fig. 10c-d) are of very moderate magnitude, within 1.5 °C at 35 years, but the results highlight the notably slow rates of temperature decrease associated with grids that are more homogeneous (117x-DE, 117x-CP), presumably in relation to the absence of internal flow barriers or thief zones. After 35 years of simulation, the relative performance of the well doublets in the grids is consistent across the two types of well layouts (Fig. 10e-f).

3.4. Impact of permeability upscaling method

Regardless of grid resolution or well layout, consistent differences

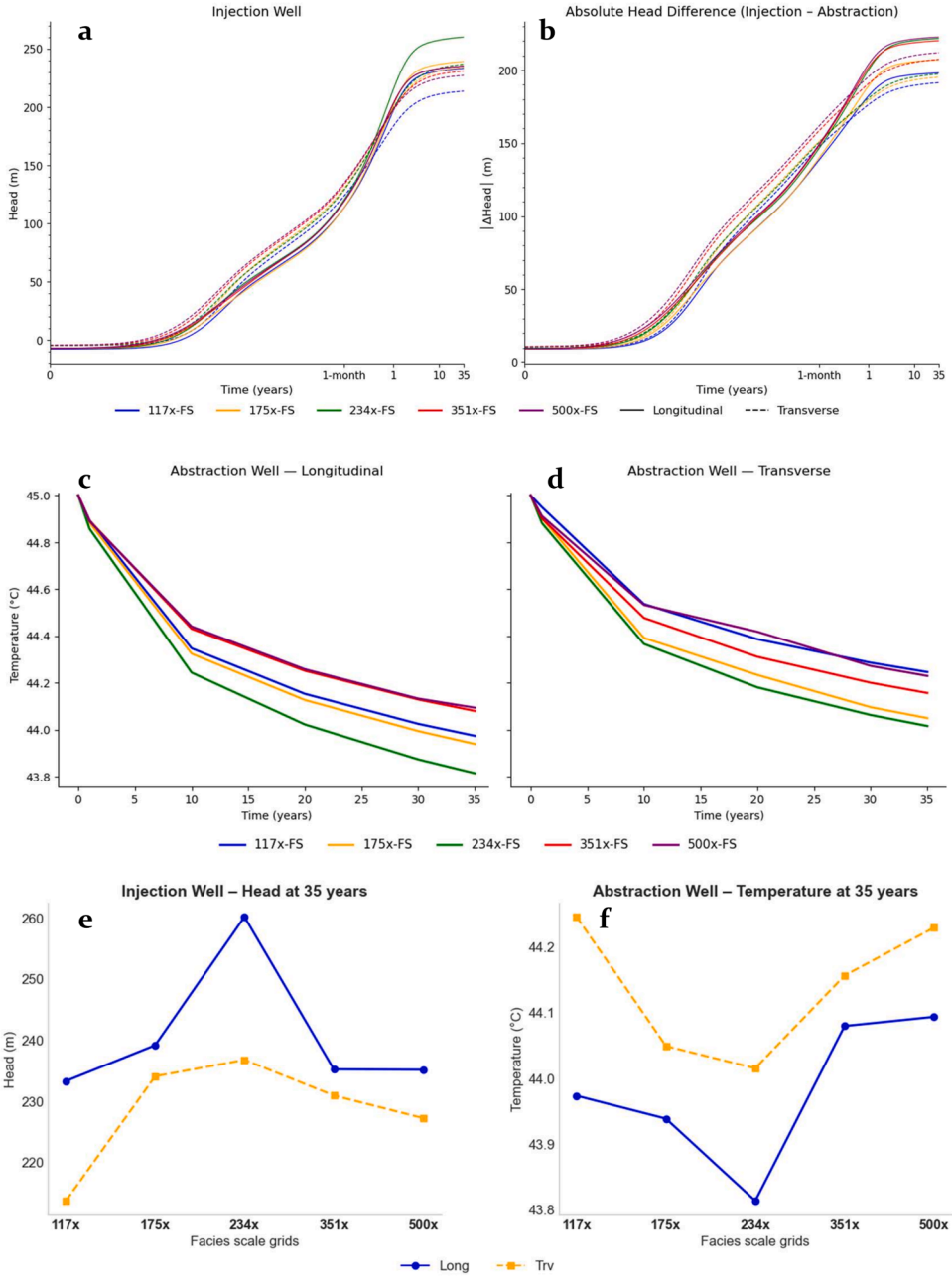

Fig. 9. Temporal evolution of (a) hydraulic head at the injection well (b) Absolute head difference (|ΔHead|) between injection and abstraction wells for longitudinal (solid lines) and transverse (dashed lines) well doublets. (c-d) Temperature history at the abstraction well for longitudinal (left) and transverse (right) well doublets. (e-f) hydraulic head at the injection well and temperature at the abstraction well after 35 years in longitudinal (solid lines, 'Long') and transverse (dashed line, 'Trv') well doublets for six grid resolutions.

are seen across facies-scale grids for which permeability values are assigned using different permeability-upscaling methods (Fig. 11). At 117x resolution, values of injector heads and absolute head differences vary widely across the different simulations, with those run on AU and FBU grids showing the lowest hydraulic heads (Fig. 11a-b). Consistently, the temperature decline at the producer is slower for simulations run on FBU and AU grids compared to those for GU and HU (Fig. 11c-d). At 500x resolution, the spread between upscaling methods narrows substantially. In this case, the injector pressure and absolute head differences increase from AU, through GU, to HU, in both layouts, with head values systematically ~10–25 m higher for the longitudinal layout than for the transverse one (Fig. 11a-b). On average, the simulations performed on the 500x grid show a lower rate of plume advance compared to those run on 117x, but this is not observed consistently across the variably upscaled grids (Fig. 11c-d). At year 35, the influence of permeability upscaling approach on near-injector hydraulic head and production temperature is resolution-dependent, since the impact of upscaling method on dynamic simulations is highest for the lower-resolution 117x grids (Fig. 11e-f). In general, the simulations run on the grid based on flow-based upscaling exhibit values of injector pressures and production temperatures after 35 years of operation that are best approximated by the results of simulations run on grids produced via arithmetic averaging. Simulations run on grids upscaled using geometric or harmonic averaging tend to predict higher injector pressures and more rapid production temperature decline.

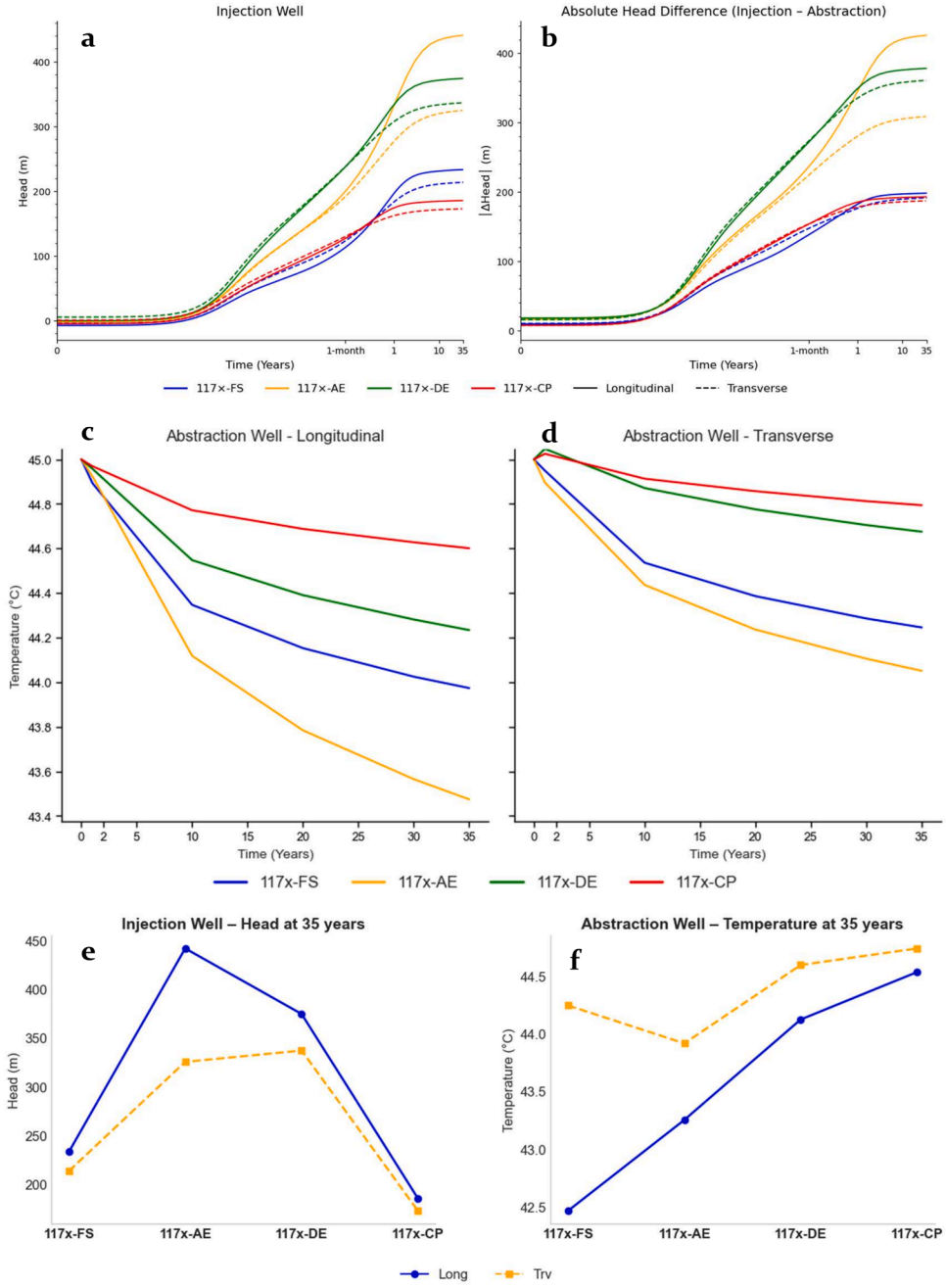

Fig. 10. Temporal evolution of hydraulic head for the four grids considering different levels of heterogeneity at a resolution of 117×104×52 cells (117x-FS: facies-scale grid, 117x-AE: architectural-element-scale grid, 117x-DE: depositional-element-scale grid, 117x-CP: grid with homogeneous channel-belt depositional element). (a-b) Pressure build-up at the injection well and absolute hydraulic head difference between injection and abstraction wells. Solid lines correspond to a longitudinal well doublet (aligned along direction of channel-belt axis), dashed lines to a transverse doublet. (c-d) Time evolution of abstraction-well temperature for longitudinal and transverse well doublets. (e-f) Injection-well hydraulic head and abstraction-well temperature after 35 years for longitudinal (solid line, 'Long') and transverse (dashed line, 'Trv') well-doublet layouts.

3.5. *Cold-water-plume shape*

For either well layout, no systematic differences in the cold-water plume geometry are seen across simulations run on grids that differ with respect to resolution or permeability upscaling method. Selected plan and cross views are shown in Fig. 12. In plan-view the planform shape of the injected water plume is delineated by near-circular to slightly elliptical isotherms; only subtle plume elongation and very limited plume roughness are observed. The simulations run on the transverse layout show a marginally more irregular plume, consistent with slightly higher values of S/V ratio, but the differences are modest.

Across the four grids embodying different hierarchies of sedimentary architectures, the simulated injected cold-water plumes are similar in size for both well layouts (Fig. 13), but some differences are seen in the geometry of the plume fronts and in plume skewness. The simulation on the homogeneous case (117x-CP) shows the most regular and smooth plume, which is approximately circular in planform. The plume in the simulation run on 117x-DE is merely slightly more irregular. The simulation run on 117x-AE highlights the impact of the channel-fill mud plug on the asymmetry of the cold-water plume, whereas that run on 117x-FS displays the impact of oriented lateral-accretion packages and associated mud drapes acting as internal flow baffles on plume

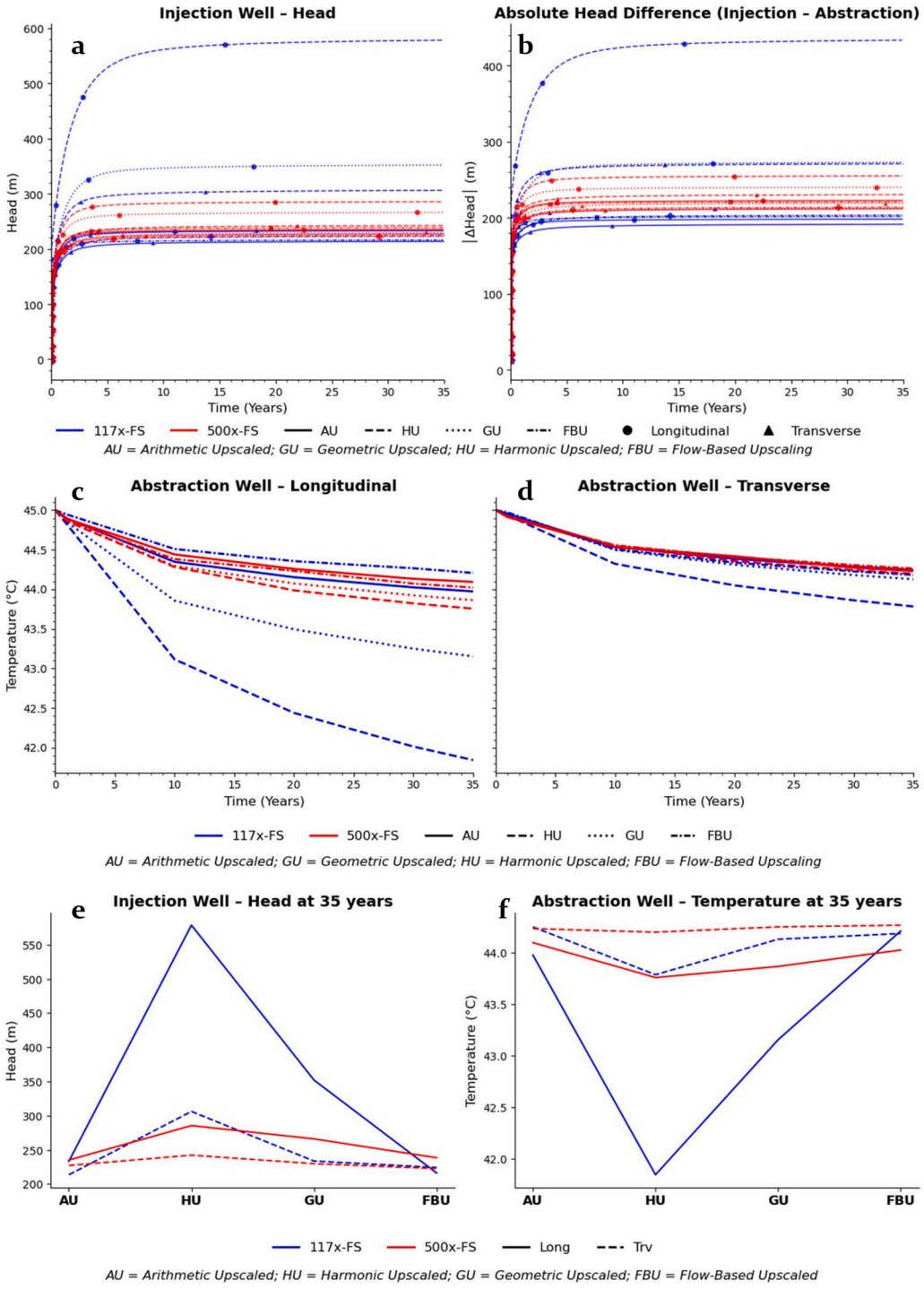

Fig. 11. Temporal evolution of hydraulic head and temperature for 117 × 104 × 52 and 500 × 104 ×52 grids based on the four different permeability upscaling schemes: arithmetic averaging (AU), geometric averaging (GU), harmonic averaging (HU), and flow-based upscaling (FBU). (a-b) Pressure build-up at the injection well (a) and absolute hydraulic head difference between injection and abstraction wells (b) for longitudinal and transverse doublets. (c-d) Abstraction well temperature for longitudinal (c) and transverse (d) well doublets. (e-f) Injection well hydraulic head (e) and abstraction well temperature (f) after 35 years for longitudinal (solid line, 'Long') and transverse (dashed line, 'Trv') well-doublet layouts.

elongation.

Fig. 14 presents the S/V values of the injected-water plumes simulated for every grid. The S/V values range from 0.185 to 0.212, underscoring the generally modest influence of model resolution and numerical upscaling procedure on plume geometry. In general, it is observed that: (i) injected plumes simulated in facies-scale grids tend to have higher S/V values than plumes in grids with simpler geological architectures; (ii) for any grid, plumes associated with transverse well-doublet layouts, i.e., with wells oriented along point-bar accretion surfaces, have systematically higher S/V values. Across all cases, S/V correlates positively with permeability heterogeneity (VDP): overall a Pearson's $r = 0.417$ is seen between the two quantities; notably, a Pearson's $r = 0.344$ is seen for longitudinal layouts and $r = 0.565$ for transverse layouts, indicating a stronger association for doublets oriented across accretion surfaces.

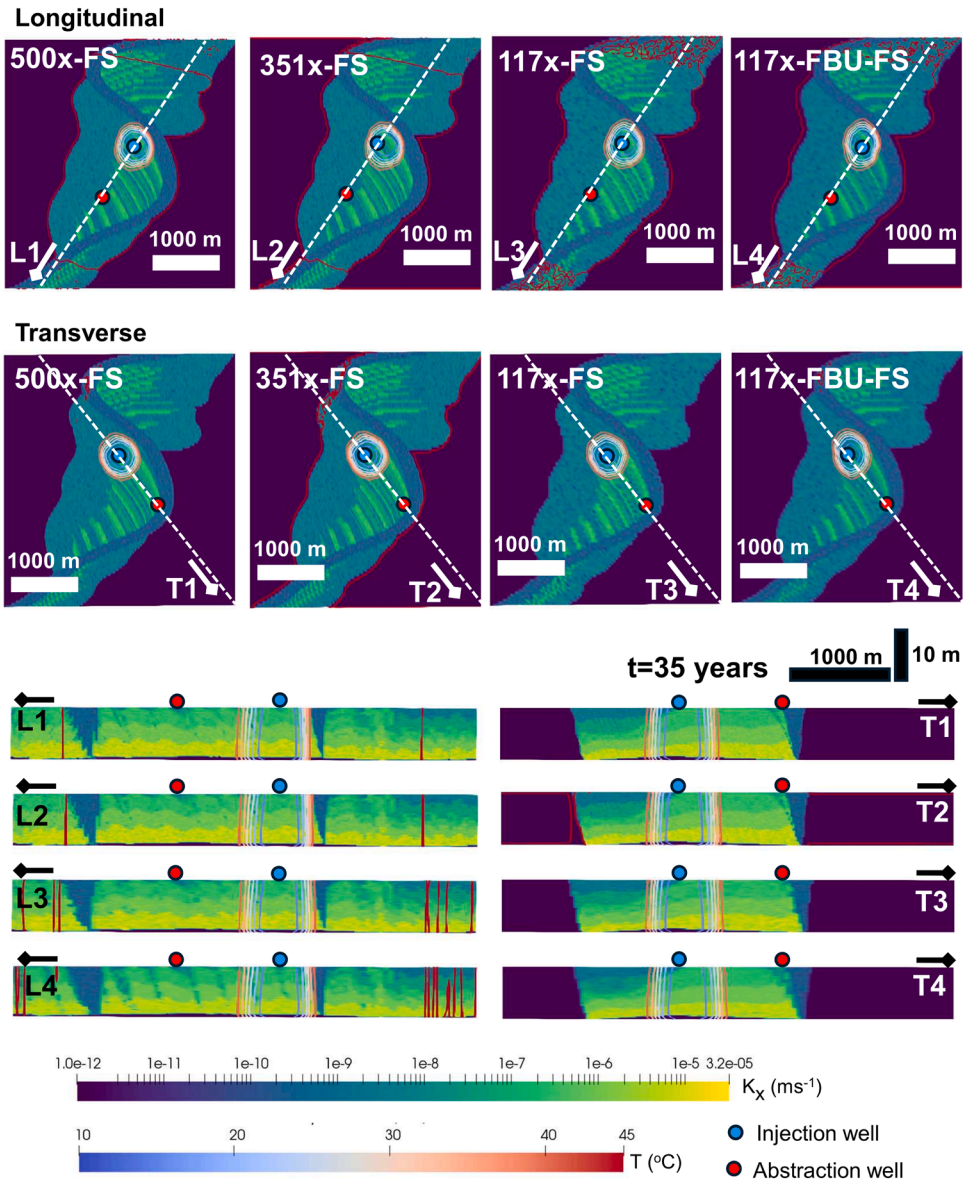

Fig. 12. Selected plan-view maps and corresponding cross-sections from cold-water plume at $t = 35$ years for longitudinal (L) and transverse (T) doublet layouts across four static grids (500x-FS, 351x-FS, 117x-FS, 117x-FBU-FS). Maps and sections are color-coded according to horizontal hydraulic conductivity (Kx). Contour colors denote temperature (10–45 °C).

4. Discussion

The numerical simulations of fluid flow and heat transport presented in this study for idealized low-enthalpy geothermal reservoirs hosted in fluvial meander-belt successions provide a systematic account of how choices regarding the ways in which sedimentary and petrophysical heterogeneities are represented in a reservoir model will affect the predicted performance of a geothermal doublet. Specifically, we focused on choices concerning the hierarchies of sedimentary architecture that one may consider, the resolution at which the corresponding sedimentary units may be rendered in a static model, and the way in which their permeability field is upscaled at the chosen resolution.

The hierarchical nature of fluvial meander-belt deposits, conceptualized in the form of lithofacies arranged into architectural elements that are themselves components of larger-scale channel-belt depositional elements (Fig. 1), is known to map onto scales of petrophysical heterogeneity that control reservoir performance (Russell et al., 2019; Willis and Sech, 2019; Willems et al., 2017a). The results of this study demonstrate that simplifying this hierarchy by omitting specific scales of heterogeneity leads to predictable changes in the simulation of both injector pressures and thermal plume propagation.

A primary finding is the dominant role of macro-scale architecture in controlling the hydraulic response of well doublets. The highest injection pressures are consistently observed in the architectural-element scale model (117x-AE), which represents point bars and channel-fill mud plugs as internally homogeneous units (Fig. 10a and c). This outcome is likely to reflect how a simplification of the geological architecture amplifies the impact of abandoned channel fills as barriers or baffles to flow compartmentalizing sand-prone point-bar elements (Colombera et al., 2017; Donselaar and Overeem, 2008) while at the same time masking permeability characteristics associated with point-bar fining upward trends. In facies-scale models (e.g., 117x-FS), the point-bar elements, although internally heterogeneous, contain interconnected pathways of higher permeability sand-prone grid-cells representing lower-bar deposits.

Visual inspection of the plume shape (Fig. 13) and quantitative analysis of their surface-to-volume (S/V) ratios (Fig. 14) reveal that considering smaller-scale lithological heterogeneities leads to more

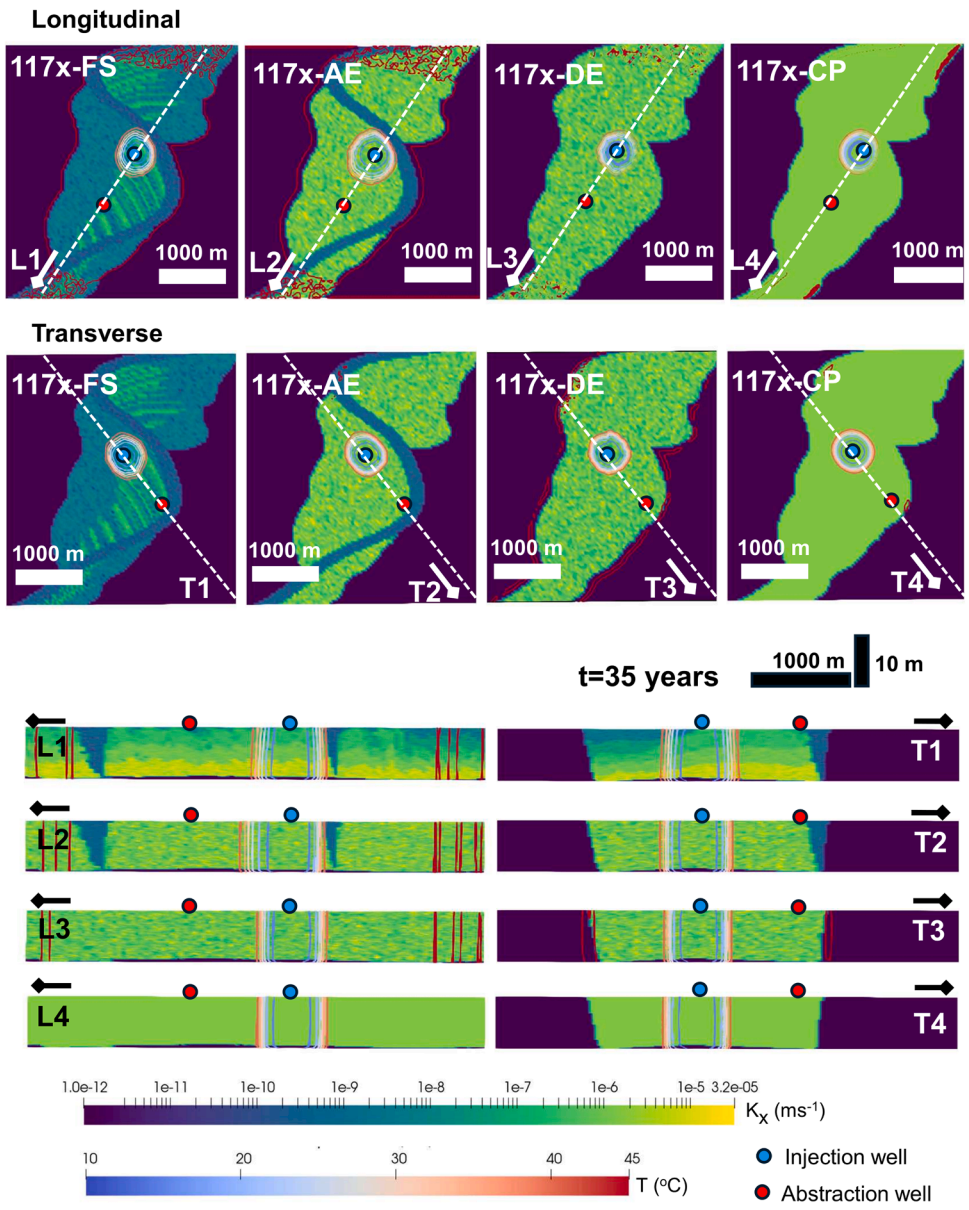

Fig. 13. Selected plan view and corresponding cross-sections from cold-water plume at $t = 35$ years for four sedimentary-hierarchy representations at fixed resolution (117×104×52): facies-scale (117x-FS), architectural-element scale (117x-AE), depositional-element with Gaussian petrophysics (117x-DE), and constant petrophysics (117x-CP). Maps and sections are color-coded according to horizontal hydraulic conductivity (Kx). Contour colors denote temperature (10–45 °C).

complex plume fronts overall, even though plume S/V ratios do not increase systematically with the resolution at which the sedimentary heterogeneities are represented. The advance of the front is locally retarded by low-permeability mud drapes and channeled through high-permeability sand-prone volumes; these features are characteristic of point-bar deposits and are typically elongated in the same direction as part of lateral-accretion packages (Bridge, 2003). Bar-front mud drapes, even when thin and discontinuous, serve as baffles that increase the effective path length of the injected fluid, thereby increasing the plume surface area (Babaei and Nick, 2019; Major et al., 2023; Montero et al., 2024). A higher surface-to-volume (S/V) ratio indicates a more complex and tortuous plume shape, which increases the total surface area for conductive heat exchange between the injected cold water and the surrounding host rock. The timing of thermal breakthrough depends critically on the orientation of elongation of the plume relative to the position of the abstraction well. If the plume is highly elongated along a direct path between the injector and producer, a higher S/V ratio is expected to be related to earlier thermal breakthrough. Conversely, a plume that spreads away from the doublet orientation taking a tortuous path due to geological heterogeneity will result in later thermal breakthrough, increasing the efficiency of heat production.

Furthermore, the results highlight how the impact of sedimentary heterogeneity on heat transport is contingent on the well-doublet orientation. For the longitudinal well layout, oriented across the dominant high-permeability flow paths, the injected fluid is forced to cross multiple lower-permeability mud drapes. By contrast, the transverse layout is arranged according to the strike direction of the accretions surfaces and the sand-prone point-bar accretion packages they delimit: the higher surface-to-volume (S/V) ratios for the transverse layout (Fig. 14) reflect enhanced plume elongation. Despite this, the decline in production temperature is faster for the longitudinal well layout regardless of the detail with which sedimentary heterogeneities are modeled, as near-injector pressures tend to be higher. This becomes especially significant in cases (FS and AE grids) where asymmetric plume propagation is enhanced by the low-permeability mud plug acting as a flow barrier (see Fig. 13). Overall, these results corroborate

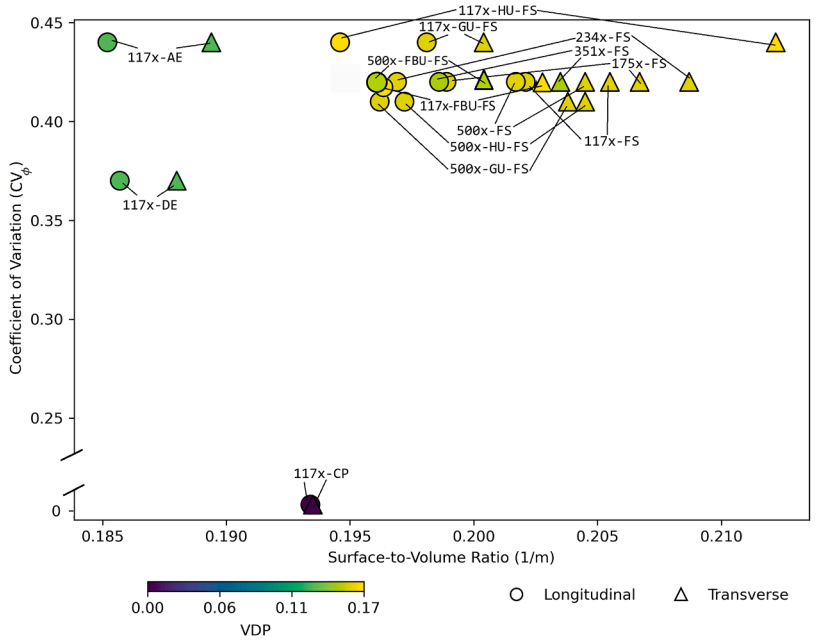

Fig. 14. Values of surface-to-volume ratio ($m - 1$) of the cold-water plume plotted against the porosity coefficient of variation (CV_ϕ) and the Dykstra–Parsons coefficient (VDP) for each grid used in this study, for both longitudinal and transverse well-doublet configurations.

previous studies that identified doublet orientation relative to paleoflow as a critical design parameter in fluvial reservoirs (Willems et al., 2017b). However, the mechanisms of meander-bend transformation—i.e., whether a point-bar element accretes via expansion, translation, and/or rotation of a meander—determines the geometry and orientation of sand-prone accretion packages and associated low-permeability mud drapes (Aghaei et al., 2024). This underscores the necessity of integrating a detailed, three-dimensional understanding of sedimentary architecture into the planning and optimization of well placement strategies.

The pressure behavior across the different heterogeneity hierarchies reveals that the preservation of high-permeability connectivity is as critical as the representation of flow barriers. Both the Architectural-Element (117x-AE) and Depositional-Element (117x-DE) models yield significantly higher injection pressures than the Facies-Scale (117x-FS) model (Fig. 10a). Since the DE model lacks discrete abandoned-channel mud plugs, this pressure increase cannot be attributed solely to large-scale compartmentalization. Instead, this behavior correlates with the complexity of the cold-water plume, quantified by the Surface-to-Volume (S/V) ratio (Fig. 14). The 117x-FS model exhibits the highest S/V ratios, reflecting a complex plume geometry where flow is channeled through interconnected high-permeability pathways—specifically the coarse-grained basal sands typical of point-bar fining-upward sequences. These pathways act as hydraulic conduits that relieve injection pressure. Conversely, the AE and DE models exhibit lower S/V ratios, indicating simpler, more compact plumes. By averaging petrophysical properties within architectural elements (AE) or distributing them stochastically without facies constraints (DE), these models effectively ignore the spatial continuity of the high-permeability streaks. Consequently, the injected fluid is forced to sweep the bulk formation rather than channeling through high-conductivity networks, resulting in a substantial overestimation of the necessary injection pressure. The slightly higher pressures in the AE model compared to the DE model can then be attributed to the additional effect of the discrete mud-plug barriers.

This points to a fundamental control of intrabody connectivity over bulk volume. Although the AE model captures large-scale compartmentalization by mud plugs, its internal homogeneity—like that of the DE model—removes the discrete, high-permeability pathways formed by coarse-grained basal point-bar sands. In the facies-scale (FS) models, these interconnected high-permeability streaks act as hydraulic 'short-circuits' or thief zones, effectively relieving near-wellbore pressure. By averaging these heterogeneities into a block mean (AE) or a Gaussian field (DE), the continuity of these conduits is compromised. Mechanistically, this forces the injected fluid to sweep the lower-permeability bulk volume rather than channeling through high-conductivity networks, resulting in a substantial overestimation of injection pressure. This aligns with the connectivity paradox described by Ringrose and Bentley (2016), where over-simplification of internal architecture often leads to overpessimistic flow predictions by masking high-permeability streaks that are common in fluvial deposits.

The process of upscaling finer-scale petrophysical properties onto a coarser grid is a necessary step in making reservoir simulation computationally tractable (Chen et al., 2003; Jenny et al., 2003). The results of this study (e.g., Fig. 11) demonstrate that the choice of upscaling method is not a mere mathematical convenience. Each method imposes a bias that emphasizes certain geological features.

For both grid resolutions and well layouts, a consistent ranking of injection pressures is seen across grids whose permeability field was upscaled in different ways: those that use harmonic averaging (HU) yield the highest pressures, followed by those using geometric averaging (GU), and then those that use arithmetic averaging (AU). This can be explained from first principles of averaging theory (Renard and de Marsily, 1997). The harmonic mean is mathematically dominated by the lowest values in a series, making it highly sensitive to low-permeability layers. In a geological context, this method effectively models thin, discontinuous mud layers as continuous, flow-perpendicular barriers, thus maximizing the predicted flow impedance. Conversely, the arithmetic mean is dominated by the highest values, which preserves the lateral continuity of high-permeability streaks and tends to underestimate the baffling effect of discontinuous shales. The geometric mean, which assigns equal weight to high and low values in logarithmic space, often provides an intermediate measure that is theoretically suited to random, uncorrelated heterogeneity but may not adequately capture the organized architecture of fluvial deposits. The clear separation of the pressure curves in Fig. 11 is therefore a direct consequence of the inherent mathematics being applied to the organized heterogeneity of the meander-belt model.

Crucially, the observation that the dynamic behavior of permeability grids based on FBU closely mimics that of grids based on arithmetic means (Fig. 11) provides a diagnostic insight into the effective flow topology of the aquifer. It indicates that the macroscopic flow behavior is dominated by continuous, high-permeability sand bodies acting in parallel, rather than being throttled by transverse barriers. This suggests that, for this specific meander-belt architecture, the 'thief zones' are sufficiently connected to bypass the baffling effects of mud drapes, a behavior consistent with the 'connected-sand' fraction concept of Jackson et al. (2003). This conclusion, which could not be reached by examining the static methods in isolation, highlights the value of FBU as a tool for diagnosing the primary flow controls in a complex model. However, it is crucial to recognize that this result is scenario-dependent; a different geological realization or well placement could easily lead to a different outcome where FBU aligns more closely with the geometric or even harmonic mean (Darban et al., 2020; Jenny et al., 2003). This behavior is consistent with theoretical bounds for flow oriented parallel to stratification (Renard and de Marsily, 1997) and indicates that the meander-belt architecture modeled here possesses high lateral sandstone connectivity. In this specific setting, continuous point-bar sands act as parallel flow conduits that bypass local baffles (Jackson et al., 2003). In other clastic aquifers where flow is more intensely forced across low-permeability barriers (series behavior), this relationship would not hold.

A key observation is that the performance gap between the different upscaling methods narrows substantially as the grid resolution is refined from 117x to 500x (Fig. 11). This convergence is a practical demonstration of the Representative Elementary Volume (REV) concept (Bear, 2013; Gómez-Hernández and Wen, 1998; Nordahl and Ringrose, 2008). At coarse grid resolutions, the cell size is large relative to the scale of the key geological heterogeneities (e.g., individual mud drapes). In this regime, the upscaling method imposes its own strong bias on how this sub-grid heterogeneity is homogenized. As the grid becomes finer, it begins to explicitly resolve these critical features. The behavior of the model becomes progressively more dependent on the explicitly gridded geology and less on the averaging assumption embedded in the upscaling scheme. Nevertheless, the system is clearly approaching a state where the effective permeability becomes a stable property of the medium, independent of the specific averaging method used, which is the definition of having reached an REV for the flow problem (Feyen and Caers, 2006; Jackson et al., 2003; Janssen et al., 2006). However, reservoir architectures tend to present mm- to cm- scale lithological heterogeneities that are not considered here, and whose impact should ideally be accounted for in a flow-based upscaling workflow through a stepwise hierarchical derivation of upscaled permeabilities; for meander-belt successions, a hierarchical application of flow-based upscaling has been shown to capture the multi-scale nature of sedimentary heterogeneity in a realistic manner (Nordahl et al., 2014).

A striking result from the grid resolution analysis is the fact that the highest values of near-injector pressure are observed for simulations run on the intermediate-resolution 234x-FS grid (Fig. 9e). This is a counter-intuitive outcome, as a monotonic convergence towards a stable solution is typically expected with grid refinement. This phenomenon can be explained by the interplay between the explicit resolution of physical features and the implicit effect of numerical dispersion. Numerical dispersion is an artifact of the finite-difference method used to solve the flow equations; it artificially smears sharp fronts in pressure and saturation over several grid cells (Bedekar et al., 2016; Harbaugh, 2005). At very coarse resolutions, such as in the 117x-FS model, this effect is pronounced. The smearing effectively averages out the hydraulic impact of small-scale flow baffles like mud drapes, leading to a lower predicted injection pressure. As the grid is refined to the 234x-FS level, numerical dispersion is reduced. The simulation run on this grid is affected by fine-scale baffles more sharply, increasing flow impedance. However, the grid is not yet fine enough to accurately resolve the tortuous, higher-permeability pathways that allow fluid to flow around these baffles. It is likely that it is the combination of these two facts that leads to an overestimation of the total flow impedance, resulting in a pressure peak. As the grid is refined further (e.g., 351x-FS and 500x-FS), the model more accurately resolves these flow pathways, the representation of flow tortuosity improves, and the solution converges towards lower pressure values. This observation serves as a critical reminder of the dangers of generalizing from a limited set of simulations and underscores the absolute necessity of conducting targeted grid-sensitivity studies that explore the interaction between grid resolution and the specific geological context of the problem at hand (Vogt et al., 2013; Wang et al., 2023). The non-monotonic pressure behavior observed during grid refinement—specifically the pressure peak at the intermediate 234x resolution—can be explained by the competing effects of explicit obstacle resolution versus numerical dispersion. However, the grid is not sufficiently fine to fully resolve the narrow high-permeability pathways around these barriers. It is only at the finest resolutions (351x, 500x) that these barrier bypass is captured, relieving the pressure.

In practice, this study demonstrates the value of geologically consistent fine-scale models (e.g., constructed using analog-constrained rule-based approaches) for the identification of which heterogeneities matter most, then adopting an upscaling approach (arithmetic/harmonic/geometric; transmissibility- or flow-based; multiscale) that demonstrably preserves those salient features, validating against fine-scale baselines to ensure that plume migration, thermal breakthrough, and well performance predicted at a coarser scale are not artifacts of over-simplification.

4.1. *Broader practical implications*

For the high-sinuosity meander-belt architectures considered in this study, the collective results of this study converge on a single, unifying principle: accurately forecasting geothermal performance in fluvial reservoirs is fundamentally a problem of preserving hydraulic connectivity across multiple geological and numerical scales. Whether the modeling choice involves simplifying architectural hierarchies, selecting an upscaling method, or defining grid resolution, the ultimate success of the model hinges on its ability to represent key sedimentary and petrophysical heterogeneities.

While this study focuses on the numerical and geological drivers of reservoir behavior, the magnitude of the simulated pressure differences has immediate practical implications for the operation of geothermal doublets. The hydraulic head differences observed between the facies-scale (FS) models and the simplified architectural-element (AE) models—often exceeding 100 m of head for the same flow rate—translate directly into operational constraints. From an engineering perspective, the high injection pressures predicted by the simplified AE and DE models would imply a significantly higher parasitic load, as pump power consumption scales linearly with the required pressure head (DiPippo, 2012; Banks, 2009). Overestimating this pressure during the exploration phase could lead to pessimistic assessments of the doublet's Net Energy Ratio (NER) or economic viability. Conversely, reliance on models that overestimate connectivity (and thus underestimate pressure) poses a risk of under-sizing surface facilities. Furthermore, correctly predicting the maximum injection pressure is critical for maintaining mechanical integrity; if the required injection pressure approaches the formation fracture gradient, the operator may be forced to throttle flow rates to avoid induced fracturing, thereby reducing the total thermal output.

Finally, it is critical to distinguish between the methodological insights of this study and its specific quantitative results. The general insight—that modeling choices regarding sedimentary hierarchy and upscaling strategy can exert a control on predicted reservoir performance that equals or exceeds the impact of grid resolution—is broadly relevant for the simulation of heterogeneous clastic aquifers. However, the observed magnitude and direction of these impacts are intrinsic to the specific connectivity patterns of high-sinuosity meander-belt architectures and the operational parameters (e.g., flow rate, well spacing)

considered here. For example, the finding that architectural-element-scale models yield the highest injection pressures is driven by the specific arrangement of point-bar sands and mud plugs in this depositional setting. Consequently, these specific quantitative trends should not be generalized to other clastic systems (e.g., successions of braided rivers or deltaic lobes) where the connectivity of high-permeability units may differ fundamentally. Practitioners should exclusively view these results in the proposed sensitivity framework.

4.2. Limitations

The study is subject to limitations that define the bounds of its applicability. Primarily, the analysis relied on a single, albeit detailed, geological realization of a meander belt. Although this model captures canonical features of this depositional environment (e.g., point bars, mud plugs), it does not capture the full spectrum of fluvial heterogeneity (e.g., braided systems, anastomosing rivers, or varying net-to-gross ratios). Consequently, the quantitative results regarding pressure magnitudes and thermal breakthrough times should be interpreted as specific to this architectural style, rather than being universally applicable to all fluvial geothermal reservoirs. The analysis was based on a single, albeit detailed, geological model. Meander-belt successions exhibit significant variability, but the computational demands of the flow-based upscaling workflow (up to approximately 380 h per grid) necessitated a pragmatic approach to enable a controlled comparison of numerical schemes. The impact of variability of facies architecture was the primary focus of a related study (Aghaei et al., 2024). The importance of variability in petrophysical properties across multiple stochastic realizations has not been explicitly quantified in this study; nevertheless, such differences are expected to have a minor impact relative to modeling choices, because petrophysical contrasts are dominated by differences between facies types rather than the internal variability within individual facies units, in the modelled scenario.

A significant limitation in the applicability of the results is the diffusion-dominated regime caused by the low flow-rate assumption, which cannot be generalized to systems operating at higher Péclet numbers. In geothermal operations with higher flow rates (and thus higher Péclet numbers), advection would dominate, making geological heterogeneity far more critical for production-temperature predictions. At such higher rates, the role of sedimentary heterogeneity in governing thermal breakthrough would be significantly amplified compared to the results observed in this study.

Finally, because the study focuses on an idealized case, validation based on history matching was not possible.

5. Conclusions

Predicting geothermal performance in fluvial reservoirs is fundamentally a problem of preserving hydraulic connectivity across multiple scales. This study shows that key modeling choices—grid resolution, upscaling methodology, and level of geological detail—have an impact on predicted geothermal doublet behavior, particularly on injection pressures. By contrast, the impact of all these choices on production temperatures is relatively modest, with a total variation of less than 2 °C over a 35-year period across all models. This limited effect is likely due to the impact of thermal diffusion under conditions of limited flow rate, in a scenario where potential variations in well deliverability have not been considered. Nonetheless, within the context of the modeled meander-belt architecture, some general implications can be derived that can be considered when modeling low-enthalpy geothermal reservoirs hosted in heterogenous siliciclastic successions: (i) the impact of omitting fine-scale facies heterogeneities is not readily predictable, since disregarding lithological variability may amplify the hydraulic impact of larger-scale features that may form flow barriers while simultaneously masking vertical and horizontal trends in permeability heterogeneity; (ii) systematic differences in plume shape between longitudinal and transverse well-doublet layouts underscore the importance of well orientation and position relative to aspects of geological architecture (e.g., flow baffles with preferential orientation); (iii) predicted well-doublet performance metrics do not vary systematically as a function of the resolution of the static model grids; (iv) the predicted well-doublet performance does not converge monotonically with grid refinement due to the decoupling of barrier resolution and connectivity resolution, a behavior modelers should be wary of when refining grids in heterogeneous reservoirs; (v) upscaling methods based on cell averaging return predicted near-injection pressures that decrease consistently from harmonic, through geometric, to arithmetic averaging; (vi) flow-based upscaling returns dynamic models that align closely with those run on grids upscaled by arithmetic averaging, suggesting that for this specific context, the bulk hydraulic behavior is dominated by the connectivity of higher-permeability, sand-prone volumes; (vii) performance differences between simulations of grids based on different upscaling methods decrease with increasing grid resolution, as REVs tend to be approximated.

Declaration of generative AI and AI-assisted technologies in the writing process

During the preparation of this work the author(s) used ChatGPT and Gemini in order to improve the readability, grammar, and descriptive clarity of the manuscript text and figure captions. After using these tools/services, the author(s) reviewed and edited the content as needed and take(s) full responsibility for the content of the published article.

Data availability

Data will be made available on request.

CRediT authorship contribution statement

Hamed Aghaei: Writing – review & editing, Writing – original draft, Visualization, Validation, Software, Resources, Methodology, Investigation, Formal analysis, Data curation, Conceptualization. **Luca Colombera:** Writing – review & editing, Writing – original draft, Visualization, Validation, Supervision, Software, Resources, Project administration, Methodology, Investigation, Funding acquisition, Formal analysis, Data curation, Conceptualization. **Na Yan:** Writing – review & editing, Software, Data curation. **Nigel P. Mountney:** Writing – review & editing, Supervision, Project administration, Funding acquisition. **Odd Andersen:** Writing – review & editing, Software. **Andrea Di Giulio:** Writing – review & editing, Funding acquisition.

Declaration of competing interest

The authors declare that they have no known competing financial interests or personal relationships that could have appeared to influence the work reported in this paper.

Acknowledgments

We thank the FRG-ERG-SMRG sponsors, and in particular the companies sponsoring phase six (AkerBP, ENI, Equinor, Murphy, Oxy), for financial support of the research group. Part of this work has also been supported by a PRIN 2022 PNRR grant (P2022PHWM4) funded by the European Union – Next Generation EU, Mission 4 Component 1, CUP: F53D23012440001. Additional financial support has been provided by the University of Pavia through the Fondo Ricerca e Giovani 2023. We also thank Daniel Feinstein for his useful feedback and suggestions. Two anonymous reviewers are thanked for their constructive criticism, which has improved the article.

Appendix A

Table 2
Hydraulic and thermal parameters used to construct the models in this study.

Parameter	Grid	Value
Dimensions (length x width x height, m)	All grids	5382 × 4784 × 110
Grid cells (columns × rows × layers, -)	117x-FS, 117x-AE, 117x-DE, 117x-CP	117 × 104 × 52
	117x-HU-FS, 117x-GU-FS, 117x-FBU-FS	
	175x-FS	175 × 104 × 52
	234x-FS	234 × 104 × 52
	351x-FS	351 × 104 × 52
	500x-FS	500 × 104 × 52
	500x-HU-FS, 500x-GU-FS, 500x-FBU-FS	
Cell (MODFLOW layer) thickness (m)	All grids	0.2
Horizontal cell size (m)	117x-FS, 117x-AE, 117x-DE, 117x-CP	46
	117x-HU-FS, 117x-GU-FS, 117x-FBU-FS	
	175x-FS	30.75
	234x-FS	23
	351x-FS	15.33
	500x-FS	10.76
	500x-HU-FS, 500x-GU-FS, 500x-FBU-FS	
Horizontal hydraulic conductivity, Kx (m s^{-1}), min-max (average)	117x-FS	1.00e e-12 – 3.18e-05 (5.33e-07)
	117x-AE	1.00e e-12 – 1.33e-04 (3.13e-07)
	117x-DE	1.00e e-12 – 1.35e-04 (2.97e-07)
	117x-CP	1.00e e-12 – 1.58e-06 (2.98e-07)
	117x-GU-FS	1.00e e-12 – 2.80e-05 (4.28e-07)
	117x-HU-FS	1.00e e-12 – 2.79e-05 (3.66e-07)
	117x-FBU-FS	1.00e e-12 – 2.79e-05 (3.66e-07)
	175x-FS	1.00e e-12 – 3.19e-05 (5.26e-07)
	234x-FS	1.00e e-12 – 3.18e-05 (5.23e-07)
	351x-FS	1.00e e-12 – 3.18e-05 (5.20e-07)
	500x-FS	1.00e e-12 – 3.20e-05 (5.20e-07)
	500x-GU-FS	1.00e e-12 – 3.17e-05 (4.88e-07)
	500x-HU-FS	1.00e e-12 – 3.17e-05 (4.72e-07)
	500x-FBU-FS	1.00e e-12 - 3.14e-05 (4.73e-07)
Horizontal hydraulic conductivity, Ky (m s^{-1}), min-max (average)	All grids (except 117x-FBU-FS and 500x-FBU-FS)	Kx
	117x-FBU-FS	1e-12 – 2.80e-05 (5.14e-07)
	500x-FBU-FS	1e-12 - 3.14e-05 (5.15e-07)
Vertical hydraulic conductivity, Kz (m s^{-1})	All grids (except 117x-FBU-FS and 500x-FBU-FS)	Kx/10
	117x-FBU-FS and 500x-FBU-FS	Ky/10
Specific storage (m^{-1})	All grids	1E-5
Porosity, ϕ (–), min-max (average)	117x-FS	0.01 – 0.33 (0.05)
	117x-AE	0.01 – 0.32 (0.04)
	117x-DE	0.01 – 0.32 (0.04)
	117x-CP	0.01 – 0.13 (0.03)
	117x-GU-FS	0.01 – 0.30 (0.05)
	117x-HU-FS	0.01 – 0.30 (0.05)
	117x-FBU-FS	0.01 – 0.33 (0.05)
	175x-FS	0.01 – 0.33 (0.05)
	234x-FS	0.01 – 0.33 (0.05)
	351x-FS	0.01 – 0.33 (0.05)
	500x-FS	0.01 – 0.33 (0.05)
	500x-GU-FS	0.01 – 0.32 (0.05)
	500x-HU-FS	0.01 – 0.32 (0.05)
	500x-FBU-FS	0.01 - 0.33 (0.05)
Dispersivity (m)	All grids	0
Water density (kg m^{-3})		1000
Water volumetric heat capacity (M J m^{-3} K^{-1})		4.18
Water thermal conductivity (W m^{-1} K^{-1})		0.607
Solid density (kg m^{-3}) – Sand-prone/Mud-prone		2640/2200
Solid volumetric heat capacity (M J m^{-3} K^{-1}) – Sand-prone/Mud-prone		2.2/2.25
Solid thermal conductivity (W m^{-1} K^{-1}) – Sand-prone/Mud-prone		3.6/2
Bulk thermal diffusion coefficient. Db (m^{-2} s), min-max (average)	117x-FS	6.47e-07 – 1.53e-06 (1.00e-06)
	117x-AE	6.47e-07 – 1.59e-06 (9.50e-07)
	117x-DE	6.47e-07 – 1.59e-06 (9.49e-07)
	117x-CP	7.93e-07 – 1.45e-06 (9.62e-07)
	117x-GU-FS	7.75e-07 – 1.57e-06 (1.01e-06)
	117x-HU-FS	7.75e-07 – 1.57e-06 (1.01e-06)
	117x-FBU-FS	6.47e-07 – 1.53e-06 (1.00e-06)
	175x-FS	6.46e-07 – 1.53e-06 (1.00e-06)
	234x-FS	6.46e-07 – 1.53e-06 (1.00e-06)
	351x-FS	6.47e-07 – 1.53e-06 (1.00e-06)
	500x-FS	6.46e-07 – 1.53e-06 (1.00e-06)

(*continued on next page*)

Table 2 (*continued*)

Parameter	Grid	Value
	500x-GU-FS	7.57e-07 – 1.57e-06 (1.00e-06)
	500x-HU-FS	7.57e-07 – 1.57e-06 (1.00e-06)
	500x-FBU-FS	6.46e-07 - 1.53e-06 (1.06e-06)
Thermal distribution coefficient, Kd (m^{-3} kg) – Sand-prone/Mud-prone	Sand-prone facies	2.1E-4
	Mud-prone facies	2.6E-4
Bulk density (kg m^{-3}), min-max (average)	117x-FS	1812 – 2525 (2229)
	117x-AE	1811 – 2588 (2207)
	117x-DE	1812 – 2590 (2205)
	117x-CP	2046 – 2430 (2218)
	117x-GU-FS	2017 – 2560 (2232)
	117x-HU-FS	2017 – 2560 (2232)
	117x-FBU-FS	1810 – 2530 (2230)
	175x-FS	1810 – 2524 (2230)
	234x-FS	1810 – 2525 (2230)
	351x-FS	1812 – 2525 (2230)
	500x-FS	1810 – 2525 (2230)
	500x-GU-FS	1988 – 2569 (2231)
	500x-HU-FS	1988 – 2569 (2231)
	500x-FBU-FS	1810 – 2525 (2230)
Flow rate (m^3 s^{-1})	All grids	0.003
Simulation time (yr)		35
Well spacing (m)		1050
Injection temperature (°C)		10
Background reservoir temperature (°C)		45
Hydraulic gradient (-)		0.003

Data availability

Data will be made available on request.

References

Aghaei, H., Colombera, L., Yan, N., Mountney, N.P., Bernagozzi, G., Di Giulio, A., 2024. Impact of fluvial meander-belt sedimentary heterogeneity on the efficiency of low-enthalpy geothermal doublets: heat-transport simulations of forward stratigraphic models. Geoenergy 2 (1), geoenergy2024-024. https://doi.org/10.1144/geoenergy2024-024.

Almeida, A.S., Journel, A.G., 1994. Joint simulation of multiple variables with a Markov-type coregionalization model. Math. Geol. 26 (5), 565–588.

Alsop, D.B., Al Ghammari, M., Al Abri, A., Al Mahrooqi, A., Al Rawahi, H., Salem, H., 2014. Reservoir Architecture of the Gharif Formation Outcrops in the Southern Huqf area, Sultanate of Oman, 387. Geological Society, London, pp. 111–133. https://doi.org/10.1144/SP387.8. Special Publications.

Babaei, M., Nick, H.M., 2019. Performance of low-enthalpy geothermal systems: interplay of spatially correlated heterogeneity and well-doublet spacings. Appl. Energy 253, 113569.

Banks, D., 2009. An introduction to 'thermogeology' and the exploitation of ground source heat. Q. J. Eng. Geol. Hydrogeol. 42 (3), 283–293. https://doi.org/10.1144/1470-9236/08-077.

Barker, J.W., Thibeau, S., 1997. A critical review of the use of pseudorelative permeabilities for upscaling. SPE Reserv. Eng. 12 (02), 138–143.

Bear, J., 2013. Dynamics of Fluids in Porous Media. Courier Corporation.

Bedekar, V., Morway, E.D., Langevin, C.D., Tonkin, M.J., 2016. MT3D-USGS version 1: a US Geological Survey release of MT3DMS updated with new and expanded transport capabilities for use with MODFLOW (2328-7055). Geological Survey Techniques and Methods. V. Reston, pp. 6–A53. Issue.

Blum, M., Martin, J., Milliken, K., Garvin, M., 2013. Paleovalley systems: insights from Quaternary analogs and experiments. Earth-Sci. Rev. 116, 128–169.

Bridge, J.S., 2003. Rivers and floodplains: forms, processes, and Sedimentary Record. John Wiley & Sons.

Chen, J., Jiang, F., 2015. Designing multi-well layout for enhanced geothermal system to better exploit hot dry rock geothermal energy. Renew. Energy 74, 37–48. https://doi.org/10.1016/j.renene.2014.07.056.

Chen, Y., Durlofsky, L.J., Gerritsen, M., Wen, X.-H., 2003. A coupled local–global upscaling approach for simulating flow in highly heterogeneous formations. Adv. Water. Resour. 26 (10), 1041–1060.

Colombera, L., Mountney, N.P., McCaffrey, W.D., 2012. A relational database for the digitization of fluvial architecture: concepts and example applications. Pet. Geosci. 18 (1), 129–140.

Colombera, L., Mountney, N.P., Medici, G., West, L.J., 2019. The geometry of fluvial channel bodies: empirical characterization and implications for object-based models of the subsurface. Am. Assoc. Pet. Geol. Bull. 103 (4), 905–929.

Colombera, L., Mountney, N.P., Russell, C.E., Shiers, M.N., McCaffrey, W.D., 2017. Geometry and compartmentalization of fluvial meander-belt reservoirs at the bar-form scale: quantitative insight from outcrop, modern and subsurface analogues. Mar. Pet. Geol. 82, 35–55.

Colombera, L., Yan, N., McCormick-Cox, T., Mountney, N.P., 2018. Seismic-driven geocellular modeling of fluvial meander-belt reservoirs using a rule-based method. Mar. Pet. Geol. 93, 553–569.

Dalla Santa, G., Galgaro, A., Sassi, R., Cultrera, M., Scotton, P., Mueller, J., Bertermann, D., Mendrinos, D., Pasquali, R., Perego, R., 2020. An updated ground thermal properties database for GSHP applications. Geothermics. 85, 101758.

Daniilidis, A., Nick, H.M., Bruhn, D.F., 2020. Interdependencies between physical, design and operational parameters for direct use geothermal heat in faulted hydrothermal reservoirs. Geothermics. 86, 101806.

Darban, A., Ghaedi, M., Qajar, J., 2020. Analysis of the impacts of relative permeability and mobility ratio on heterogeneity loss error during upscaling of geological models. Oil Gas Sci. Technol.–Rev. IFP Energ. nouv. 75, 53.

Deutsch, C.V., 1998. Fortran programs for calculating connectivity of three-dimensional numerical models and for ranking multiple realizations. Comput. Geosci. 24 (1), 69–76.

DiPippo, R., 2012. Geothermal Power plants: principles, applications, Case Studies and Environmental Impact. Butterworth-Heinemann.

Donselaar, M.E., Overeem, I., 2008. Connectivity of fluvial point-bar deposits: an example from the Miocene Huesca fluvial fan, Ebro Basin, Spain. Am. Assoc. Pet. Geol. Bull. 92 (9), 1109–1129.

Dykstra, H., Parsons, R.L., 1950. The prediction of oil recovery by water flood. Second. recovery oil U. S. 2, 160–174.

Ezekiel, J., Ebigbo, A., Arifianto, I., Daniilidis, A., Finkbeiner, T., Mai, P.M., 2022. Techno-economic performance optimization of hydrothermal doublet systems: application to the Al Wajh basin, Western Saudi Arabia. Geothermics. 105, 102532.

Ferguson, G., 2007. Heterogeneity and thermal modeling of ground water. Groundwater 45 (4), 485–490.

Feyen, L., Caers, J., 2006. Quantifying geological uncertainty for flow and transport modeling in multi-modal heterogeneous formations. Adv. Water. Resour. 29 (6), 934–949. https://doi.org/10.1016/j.advwatres.2005.08.002.

Ghinassi, M., Ielpi, A., 2015. Stratal architecture and morphodynamics of downstream-migrating fluvial point bars (Jurassic Scalby Formation, UK). J. Sediment. Res. 85 (9), 1123–1137.

Gibling, M.R., 2006. Width and thickness of fluvial channel bodies and valley fills in the geological record: a literature compilation and classification. J. Sediment. Res. 76 (5), 731–770.

Gómez-Hernández, J.J., Wen, X.H., 1998. To be or not to be multi-Gaussian? A reflection on stochastic hydrogeology. Adv. Water. Resour. 21 (1), 147–154. https://doi.org/10.1016/S0309-1708(96)00031-0.

Graham, G.H., Jackson, M.D., Hampson, G.J., 2015. Three-dimensional modeling of clinoforms in shallow-marine reservoirs: part 2. Impact on fluid flow and hydrocarbon recovery in fluvial-dominated deltaic reservoirs. Am. Assoc. Pet. Geol. Bull. 99 (6), 1083–1109. https://doi.org/10.1306/01191513191.

Gringarten, A.C., 1978. Reservoir lifetime and heat recovery factor in geothermal aquifers used for urban heating. Pure Appl. Geophys. 117 (2), 297–308.

Hamm, V., Lopez, S., 2012. Impact of fluvial sedimentary heterogeneities on heat transfer at a geothermal doublet scale. In: Proceedings of the 37th Stanford Geothermal Workshop, SGP-TR-194, Stanford, CA.

Harbaugh, A.W., 2005. MODFLOW-2005, the U.S. Geological Survey Modular Ground-Water model: the Ground-Water Flow Process, 6-A16. U.S. Department of the Interior, U.S. Geological Survey Reston, VA, USA. https://doi.org/10.3133/tm6A16.

Hartkamp-Bakker, C.A., Donselaar, M.E., 1993. Permeability patterns in point bar deposits: tertiary Loranca Basin, central Spain. In: Flint, S.S., Bryant, I.D. (Eds.), The Geological Modelling of Hydrocarbon Reservoirs and Outcrop Analogues. Blackwell Scientific Publications, pp. 157–168.

Jackson, M.D., Muggeridge, A.H., Yoshida, S., Johnson, H.D., 2003. Upscaling permeability measurements within complex heterolithic tidal sandstones. Math. Geol. 35. https://doi.org/10.1023/A:1026236401104.

Janssen, G.M.C.M., Valstar, J.R., Zee, S.E.A.T.M., 2006. Inverse modeling of multimodal conductivity distributions. Water. Resour. Res. 42 (8), W08415. https://doi.org/10.1029/2005WR004356.

Jenny, P., Lee, S., Tchelepi, H.A., 2003. Multi-scale finite-volume method for elliptic problems in subsurface flow simulation. J. Comput. Phys. 187 (1), 47–67.

Kong, Y., Pang, Z., Shao, H., Kolditz, O., 2017. Optimization of well-doublet placement in geothermal reservoirs using numerical simulation and economic analysis. Env. Earth Sci 76, 1–7.

Lake, L.W., Jensen, J.L., 1991. A review of heterogeneity measures used in reservoir characterization. Situ 15 (4), 409–439.

Lie, K.-A., 2019. An Introduction to Reservoir Simulation Using MATLAB/GNU Octave: User guide For the MATLAB Reservoir Simulation Toolbox (MRST). Cambridge University Press, Cambridge, UK; New York, NY, USA.

Lie, K.-A., Møyner, O., 2021. Advanced Modelling With the MATLAB Reservoir Simulation Toolbox. Cambridge University Press.

Mahbaz, S., Yaghoubi, A., Dehghani-Sanij, A., Sarvaramini, E., Leonenko, Y., Dusseault, M.B., 2021. Well-doublets: a first-order assessment of geothermal sedheat systems. Appl. Sci. 11 (2), 697.

Major, M., Daniilidis, A., Hansen, T.M., Khait, M., Voskov, D., 2023. Influence of process-based, stochastic and deterministic methods for representing heterogeneity in fluvial geothermal systems. Geothermics. 109, 102651.

McGowen, J., Garner, L., 1970. Physiographic features and stratification types of coarse-grained pointbars: modern and ancient examples 1. Sedimentology 14 (1–2), 77–111.

Miall, A., 2014. Fluvial Depositional Systems, 14. Springer International Publishing Switzerland.

Montero, J.M., Colombera, L., Yuste, E., Yan, N., Mountney, N.P., 2024. Assessing the impact of sedimentary heterogeneity on CO2 injection in fluvial meander-belt successions using geostatistical modelling informed by geological analogues. Int. J. Greenh. Gas Control 136, 104199.

Nordahl, K., Messina, C., Berland, H., Rustad, A.B., Rimstad, E., 2014. Impact of multiscale modelling on predicted porosity and permeability distributions in the fluvial deposits of the Upper Lunde Member (Snorre Field, Norwegian Continental Shelf). Mar. Pet. Geol. 57, 293–309.

Nordahl, K., Ringrose, P.S., 2008. Identifying the representative elementary volume for permeability in heterolithic deposits using numerical rock models. Math. Geosci. 40 (2), 163–182. https://doi.org/10.1007/s11004-008-9182-4.

Possemiers, M., Huysmans, M., Batelaan, O., 2015. Application of multiple-point geostatistics to simulate the effect of small-scale aquifer heterogeneity on the efficiency of aquifer thermal energy storage. Hydrogeol. J. 23 (5), 971–983.

Pranter, M.J., Ellison, A.I., Cole, R.D., Patterson, P.E., 2007. Analysis and modeling of intermediate-scale reservoir heterogeneity based on a fluvial point-bar outcrop analog, Williams Fork Formation, Piceance Basin, Colorado. Am. Assoc. Pet. Geol. Bull. 91 (7), 1025–1051.

Renard, P., de Marsily, G., 1997. Calculating equivalent permeability: a review. Adv. Water. Resour. 20 (5–6), 253–278. https://doi.org/10.1016/S0309-1708(96)00050-4.

Ringrose, P.S., Bentley, M.J., 2016. Reservoir Model Design: A Practitioner's Guide, 2. Springer.

Rühaak, W., Guadagnini, A., Geiger, S., Bär, K., Gu, Y., Aretz, A., Homuth, S., Sass, I., 2015. Upscaling thermal conductivities of sedimentary formations for geothermal exploration. Geothermics. 58, 49–61.

Russell, C.E., Mountney, N.P., Hodgson, D.M., Colombera, L., 2019. A novel approach for prediction of lithological heterogeneity in fluvial point-bar deposits from analysis of meander morphology and scroll-bar pattern. In: Ghinassi, M., Colombera, L., Mountney, N.P., Reesink, A.J., Bateman, M. (Eds.), Fluvial Meanders and Their Sedimentary Products in the Rock Record. John Wiley & Sons, pp. 385–418. https://doi.org/10.1002/9781119424437.ch15.

Sommer, W., Valstar, J., van Gaans, P., Grotenhuis, T., Rijnaarts, H., 2013. The impact of aquifer heterogeneity on the performance of aquifer thermal energy storage. Water. Resour. Res. 49 (12), 8128–8138.

Tyler, N., Finley, R.J., 1991. Architectural controls on the recovery of hydrocarbons from sandstone reservoirs. N. In: Miall, A.D.a.T. (Ed.), The Three-dimensional Facies Architecture of Terrigenous Clastic Sediments and Its Implications for Hydrocarbon Discovery and Recovery, The Three-dimensional Facies Architecture of Terrigenous Clastic Sediments and Its Implications for Hydrocarbon Discovery and Recovery, 3. Society for Sedimentary Geology.

Vogt, C., Iwanowski-Strahser, K., Marquart, G., Arnold, J., Mottaghy, D., Pechnig, R., Gnjezda, D., Clauser, C., 2013. Modeling contribution to risk assessment of thermal production power for geothermal reservoirs. Renew. Energy 53, 230–241.

Wang, Y., Voskov, D., Daniilidis, A., Khait, M., Saeid, S., Bruhn, D., 2023. Uncertainty quantification in a heterogeneous fluvial sandstone reservoir using GPU-based Monte Carlo simulation. Geothermics. 114, 102773.

Willems, C.J., Nick, H.M., Donselaar, M.E., Weltje, G.J., Bruhn, D.F., 2017a. On the connectivity anisotropy in fluvial Hot Sedimentary Aquifers and its influence on geothermal doublet performance. Geothermics. 65, 222–233.

Willems, C.J., Nick, H.M., Weltje, G.J., Bruhn, D.F., 2017b. An evaluation of interferences in heat production from low enthalpy geothermal doublets systems. Energy 135, 500–512.

Willis, B.J., Sech, R.P., 2019. Emergent facies patterns within fluvial channel belts. In: Ghinassi, M., Colombera, L., Mountney, N.P., Reesink, A.J., Bateman, M. (Eds.), Fluvial Meanders and Their Sedimentary Products in the Rock Record. John Wiley & Sons, pp. 509–542. https://doi.org/10.1002/9781119424437.ch19.

Yan, N., Colombera, L., Mountney, N.P., 2021. Controls on fluvial meander-belt thickness and sand distribution: insights from forward stratigraphic modelling. Sedimentology 68 (5), 1831–1860.

Yan, N., Mountney, N.P., Colombera, L., Dorrell, R.M., 2017. A 3D forward stratigraphic model of fluvial meander-bend evolution for prediction of point-bar lithofacies architecture. Comput. Geosci. 105, 65–80.

Zinsalo, J.M., Lamarche, L., Raymond, J., 2021. Design and optimization of multiple wells layout for electricity generation in a multi-fracture enhanced geothermal system. Sustain. Energy Technol. Assess. 47, 101365. https://doi.org/10.1016/j.seta.2021.101365.